Materials Science and Engineering R xxx (2013) xxx–xxx

Contents lists available at SciVerse ScienceDirect

Materials Science and Engineering R

journal homepage: www.elsevier.com/locate/mser

Review

Polymer/carbon based composites as electromagnetic interference (EMI) shielding materials

Jean-Michel Thomassin [a,*], Christine Jérôme [a], Thomas Pardoen [b,c], Christian Bailly [b,c,d], Isabelle Huynen [b,e,*], Christophe Detrembleur [a,*]

[a] University of Liege (ULg), Department of Chemistry, Center for Education and Research on Macromolecules (CERM), Sart-Tilman B6A, 4000 Liege, Belgium
[b] Research Center in Architectured and Composite Materials, ARCOMAT, Université Catholique de Louvain, B-1348 Louvain-la-Neuve, Belgium
[c] Institute of Mechanics, Materials and Civil Engineering (iMMC) , Université Catholique de Louvain, B-1348 Louvain-la-Neuve, Belgium
[d] Institute of Condensed Matter and Nanosciences (IMCN) , Université Catholique de Louvain, B-1348 Louvain-la-Neuve, Belgium
[e] Information and Communications Technologies, Electronics and Applied Mathematics (ICTEAM) , Université Catholique de Louvain, B-1348 Louvain-la-Neuve, Belgium

ARTICLE INFO

Article history:
Available online xxx

ABSTRACT

The extensive development of electronic systems and telecommunications has lead to major concerns regarding electromagnetic pollution. Motivated by environmental questions and by a wide variety of applications, the quest for materials with high efficiency to mitigate electromagnetic interferences (EMI) pollution has become a mainstream field of research. This paper reviews the state-of-the-art research in the design and characterization of polymer/carbon based composites as EMI shielding materials. After a brief introduction, in Section 1, the electromagnetic theory will be briefly discussed in Section 2 setting the foundations of the strategies to be employed to design efficient EMI shielding materials. These materials will be classified in the next section by the type of carbon fillers, involving carbon black, carbon fiber, carbon nanotubes and graphene. The importance of the dispersion method into the polymer matrix (melt-blending, solution processing, etc.) on the final material properties will be discussed. The combination of carbon fillers with other constituents such as metallic nanoparticles or conductive polymers will be the topic of Section 4. The final section will address advanced complex architectures that are currently studied to improve the performances of EMI materials and, in some cases, to impart additional properties such as thermal management and mechanical resistance. In all these studies, we will discuss the efficiency of the composites/devices to absorb and/or reflect the EMI radiation.

Abbreviations: μm, micrometer; 3D, three dimensional; ABS, acrylonitrile-butadiene-styrene copolymer; Ag, silver; ASTM, American Society for Testing and Material; BR, butyl rubber; CB, carbon black; cm, centimeter; CNF, carbon nanofiber; CNP, carbon nanoparticle; CNT, carbon nanotube; CO_2, carbon dioxide; Db, decibels; DC, direct current; E, electrical field; EM, electromagnetic; EMA, poly(ethylene-co- methylacrylate); EMI, electromagnetic interference; EMT, Effective Medium Theory; EPDM, ethylene-propylene-diene monomer rubber; EVA, poly(ethylene-co-vinyl acetate); GFRC, glass fiber reinforced cement; GHz, GigaHertz; GS, graphene sheet; H, magnetic field; HDPE, high density polyethylene; HIPS, high impact polystyrene; LDPE, low density polyethylene; LLDPE, linear low density polyethylene; MHz, MegaHertz; mm, millimeter; MMA, methyl methacrylate; MWNT, multi-walled carbon nanotube; NBR, nitrile butadiene rubber; Ni, nickel; nm, Nanometer; P(Vac-co-VA), poly(vinyl acetate-co-vinyl alcohol); P3HT, poly(3-hexylthiophene); PANI, polyaniline; Pc, percolation threshold; PC, polycarbonate; PCL, polycaprolactone; PDMS, poly(dimethylsiloxane); PE, polyethylene; PEEK, poly(ether ether ketone); PEO, poly(ethylene oxide); PET, poly(ethylene terephtalate); PEtOc, poly(ethylene-co-octene); Pin, incident power; PLLA, poly(L-lactide); PMMA, poly(methyl methacrylate); PMTT, poly(trimethylene terephtalate); POSS, polyhedral oligomeric silsesquioxanes); Pout, transmitted power; PP, polypropylene; PPE, poly(phenylene ether); PP-g-MA, poly(propylene-graft-maleic anhydride); PPV, poly(p-phenylene-vinylene); PPY, polypyrolle; Pref, reflected power; PS, polystyrene; PUR, polyurethane; PVC, poly(vinyl chloride); PVDF, poly(vinylidene fluoride); PVOH, poly(vinyl alcohol); PVP, poly(vinylpyrrolidone); RAM, radar absorbing materials; RCS, radar cross section; RF, radio frequency; S, Siemens; SBR, styrene-butadiene rubber; SE, shielding effectiveness; SEA, shielding effectiveness by absorption; SER, shielding effectiveness by reflection; Sn, Tin; SWNT, single-walled carbon nanotube; VGCNF, vapor grown carbon nanofiber; VNA, vector network analyzer; wt%, Weight Percent; ε, dielectric constant; μ, permeability; σ, electrical conductivity.

* Corresponding authors. Tel.: +32 4 3663465; fax: +32 4 3663497.
E-mail address: christophe.detrembleur@ulg.ac.be (C. Detrembleur).

0927-796X/$ – see front matter © 2013 Elsevier B.V. All rights reserved.
http://dx.doi.org/10.1016/j.mser.2013.06.001

Contents

1. Introduction . . . 000
2. Electromagnetic theory . . . 000
2.1. Electrical properties of CNP nanocomposites . . . 000
2.2. Modeling of wave propagation in CNP composites . . . 000
3. Polymer/carbon based composites as EMI shielding materials . . . 000
3.1. Graphite and carbon black as conductive fillers . . . 000
3.2. Carbon fibers as conductive fillers . . . 000
3.2.1. Melt-mixing CNF . . . 000
3.2.2. Other dispersion methods . . . 000
3.3. Carbon nanotubes as conductive fillers . . . 000
3.3.1. Melt-mixing CNT . . . 000
3.3.2. Other dispersion methods . . . 000
3.4. Graphene sheets as conductive fillers . . . 000
3.5. Summary . . . 000
4. Combination with other kinds of fillers . . . 000
4.1. Coating the carbon filler with metallic layers . . . 000
4.2. Co-addition of metallic or metal oxide nanoparticles . . . 000
4.3. Modification with intrinsic conductive polymer . . . 000
5. Complex architectures of polymer/carbon based composites for EMI shielding . . . 000
5.1. Nanocomposite foams . . . 000
5.2. Multilayers . . . 000
5.3. Honeycombs . . . 000
6. Conclusions . . . 000
Acknowledgements . . . 000
References . . . 000

1. Introduction

Electromagnetic interferences (EMI) can be defined as conducted and/or radiated electromagnetic signals emitted by electrical circuits which, under operation, perturb proper operation of surrounding electrical equipments or cause radiative damage to living/biological species. The extensive development of gigahertz electronic systems and telecommunication devices has raised the electromagnetic pollution to a level never attained before, which justifies an active quest for novel and effective EMI shielding material solutions in a wide variety of applications. A large range of applications is concerned from commercial and scientific electronic instruments to antenna systems and military electronic devices. Another military application is stealth, devoted to the reduction of the detectability of target by canceling reflections of a radar signal incident to its surface. So-called Radar Absorbing Materials (RAM) can be processed under different forms: conductive paints or rubbers loaded with ferrite and/or carbon black particles were developed for stealth military planes by various countries (information is most often classified), while conductive foams and/or multilayered topologies are commonly used as liners for all enclosures in which reflection of waves has to be minimized, such as in anechoic chambers used as reference test environment for Electromagnetic Compatibility and ElectroMagnetic Interference (EMI) shielding certification measurements [1]. More generally, electromagnetic shielding is defined as the prevention of the propagation of electric and magnetic waves from one region to another by using conducting or magnetic materials. The shielding can be achieved by minimizing the signal passing through a system either by reflection of the wave or by absorption and dissipation of the radiation power inside the material.

Nowadays, the most common way to shield electrical circuits is by reflection owing to the use of metallic sheets. Such shielding is known since more than two centuries as the Faraday cage effect operating from DC to high frequency and based on the reorganization of electric charges in the shielding conductor in order to cancel the total electric field inside or outside the cage, depending on the position of the source. Faraday cage has no effect on magnetic field, but a similar shielding mechanism is obtained for the magnetic field at relatively low frequency when using a mu metal, that is a metal which has a very high relative permeability. As a consequence, such material is able to concentrate magnetic flux in the metal, preventing its expansion after the metal thickness [1]. Such solutions have the inconvenience of poor mechanical flexibility due to the high stiffness, high weight density, propensity to corrosion, and limited tuning of the shielding effectiveness (SE) [2]. Moreover, the electromagnetic pollution is not truly eliminated or mitigated since the electromagnetic signals are almost completely reflected at the surface of the metal sheets protecting the environment only beyond the shield. During the last two decades, a large amount of researches have been focused on the design of shielding materials which work by absorption, based on polymeric materials in order to take advantage of their lightness, low cost, easy shaping, etc. Nevertheless, most polymers possess intrinsic electrical insulating properties which make them almost transparent to electromagnetic waves. In order to circumvent this drawback, conductive nanoparticles are dispersed in appropriate concentrations within the insulating polymer matrix in order to induce the absorption of the radiation power via dissipation in the conductive particles while limiting the total reflection occurring at the surface.

Three main strategies have been investigated to process EM absorbing polymer based composites. The first one consists in the dispersion of metallic fillers, fibers [3–7] or nanoparticles [8–13] within a polymer matrix in order to increase the interaction with the electromagnetic radiation. Stainless steel fibers have been dispersed within polycarbonate [5], acrylonitrile-butadiene-styrene copolymer [14], polyphenylene ether (PPE) [4], and polypropylene [6] while the dispersion of copper fibers within an epoxy matrix has also been studied [3]. Bagwell et al. have shown that the smaller the fiber diameter, the higher the shielding effectiveness [3]. However, good dispersion, which is a

Please cite this article in press as: J.-M. Thomassin, et al., Mater. Sci. Eng. R (2013), http://dx.doi.org/10.1016/j.mser.2013.06.001

prerequisite for good EMI shielding performances, is difficult to obtain with this kind of filler. The weight increase of the material resulting from the addition of metallic fillers is another drawback. The second method relies on the blending of a conventional polymer that will ensure adequate mechanical properties of the materials with an intrinsically conductive polymer which will interact with the electromagnetic radiation. Polypyrrole (PPY) [15–18] and polyaniline (PANI) [19–25] are the most common intrinsically conductive polymers used for this application. Only a few examples are reported on composites based on poly(p-phenylene-vinylene) (PPV) [26] and poly(3-octylthiophene) [27]. The shielding properties arise from the increase in electrical conductivity by addition of the conductive polymer and are consequently dominated by reflection mechanisms due to the increase of the level of impedance mismatch with air, as discussed in the second section of this review [18,21]. The poor processability of conductive polymers and the high filling levels needed for acceptable performances are the two main drawbacks of these composites. The third strategy is by far the most developed and consists in dispersing carbon based electrically conductive fillers within polymer matrices. Carbon black and carbon fiber have been the first carbon fillers to be envisioned but recently, carbon particles with very high aspect ratio, i.e. carbon nanotubes and graphene sheets, have received a lot of attention from the scientific community.

A recent review has been devoted to these different polymer composites for EMI shielding application [2]. While the two first strategies have been well documented, the present contribution has a specific and detailed focus on the carbon based composites, especially on the new extensively studied carbon nanotubes and graphene sheets. Note also that another review has been dedicated to the design of microwave absorber based on carbon particle filled polymer composites [28]. This review focusses on a narrow range of materials with very high absorption coefficients and, consequently, numerous studies were not reported.

The present paper is divided into five sections. In the next section (Section 2), we will describe the electromagnetic theory and the main parameters that influence the final electromagnetic properties of materials. Then, the different materials envisioned for reaching high EM absorption performances will be described and classified according to the nature of the carbon fillers, i.e. carbon black (Section 3.1), carbon fibers (Section 3.2), carbon nanotubes (Section 3.3) and graphene sheets (Section 3.4). Section 4 will be devoted to the combination and/or comparison of these carbon based loadings with other fillers, mainly metallic particles. Finally, various architectures of carbon-based EMI shielding composites will be described in Section 5.

At this stage, it is important to note that a direct comparison of the performances/properties reported among different publications is generally not realistic since the EMI measurements were not performed with the same methods, and/or within the same frequency ranges and/or, more importantly, with the same sample thickness. However, we will report the shielding effectiveness resulting from different strategies while specifying the investigated frequency and the material thickness in order to draw tendencies about the best roads toward the enhancement of the shielding performances of polymer/carbon particles composites.

2. Electromagnetic theory

The present section reports on state-of-the art EM modeling of CNP nanocomposites in view of predicting their electromagnetic shielding properties. Section 2.1 sets up the electrical properties of CNP nanocomposites, at DC and microwave frequencies, while Section 2.2 establishes the generalized formalism taking into account the various mechanisms involved in the EMI shielding and related EM absorption mechanisms.

2.1. Electrical properties of CNP nanocomposites

The electrical parameter of interest for shielding and absorption of EM waves is the complex permittivity $\varepsilon_r' = \varepsilon' - j\varepsilon''$, or, equivalently, the dielectric constant (ε') and the conductivity ($\sigma' = -\omega\varepsilon_0\varepsilon''$) of the nanocomposite. The relevant dual magnetic parameter is the complex permeability noted $\mu_r = \mu' - j\mu''$. Throughout the paper, only the real part σ' of the conductivity is discussed, considering that the imaginary part noted σ" could be obtained from the frequency dependence of the real part of the permittivity via the equivalent definition $\sigma'' = \omega\varepsilon_0\varepsilon'$.

A wide variety of parameters impact the electrical conductivity of nanocomposite polymers: the type(s) of polymer(s) composing the matrix, the properties of the CNPs themselves (aspect-ratio, specific surface area, surface conductivity, etc.), but also their dispersion and interactions with the host matrix [29]. The DC conductivity of nanocomposites usually exhibits a non-linear sharp increase when increasing the CNP concentration (as exemplified in Fig. 2.1 for epoxy-nanocomposites loaded with carbon nanotubes (CNTs) as conducting fillers), denoting the transition from isolated to interconnected (or "percolating") configuration of conductive particles dispersed in the matrix. Close to this percolation threshold, the DC electrical conductivity σ_0 of the nanocomposite versus CNP concentration follows a power law:

$$\sigma_0 \propto (p - p_c)^t \quad p \geq \sim p_c \tag{2.1}$$

where p is the concentration of the conductive filler, p_c is the percolation threshold, while the exponent t depends on the dimensionality of the system [30,31]: $t \sim 1.3$ in two-dimensional systems, and varies between 1.6 and 2 for 3D systems. The modeling of the conductivity of insulator-conductor systems (not restricted to CNPs) has been thoroughly investigated since more than 40 years (see for example the pioneering work of Kirkpatrick [32], with particular interest for percolation behavior. Flandin et al. [33] reported on a corresponding power law introduced by Stauffer [34] for the DC value of dielectric constant, rewritten according to the notations in this paper as:

$$\varepsilon_r \propto |p - p_c|^s \tag{2.1bis}$$

with as theoretical value for 3D systems $s = 0.7$. Expression (2.1bis) clearly predicts a divergence of the dielectric constant value in the close vicinity of the percolation threshold. This divergence prediction was successfully confirmed for measurements by

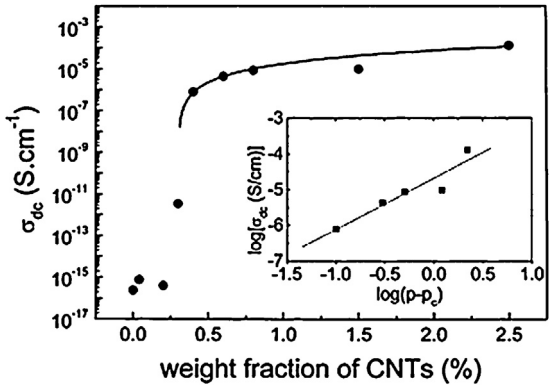

Fig. 2.1. Measured DC conductivity σ' versus CNTs weight fraction for epoxy-based nanocomposites, from [29]. The solid line is a fit to measured data, derived from a log-log fit shown in the inset, of the DC conductivity versus the difference $(p - p_c)$, and corresponding to equation (2.1). Reprinted with permission from [29]. Copyright (2003) American Chemical Society.

Flandin et al. on short fiber polypyrole composites. However, other experiments, especially related to CNT particles in polycarbonate [35], in polyimide [36,37], and even in alumina matrix, do not produce such divergence close to the percolation threshold. A tentative explanation for this absence of divergence, or equivalently an increase of dielectric constant above the percolation threshold is the presence of micro-capacitors between arms of the CNTs.

The percolation threshold depends on the aspect ratio of the conducting particles. According to the predictions by Lagarkov and Sarychev [38], and Grimmes [39], a linear decrease is expected for conducting 'sticks', or elongated inclusions. Balberg et al. [40] proposed the following relationship for a random isotropic configuration of long sticks with length L and radius r

$$\left(\frac{L}{r}\right) p_c = 3 \tag{2.2}$$

This equation, correlated with an experimental characterization of the percolation threshold p_c and an approximate knowledge of CNT geometry, can yield information on the dispersion, i.e. whether individual CNTs or bundles of nanotubes are responsible for the conduction [29]. However, CNTs inside a nanocomposite can exhibit a significantly curved shape, which degrades the conductivity of the composite [41] and induces multiple contacts between tubes. Rodney et al. proposed a computational model for the entanglement transition of network of fibers as a function of their aspect ratio [42]. The number of contacts per fiber is calculated for various aspect ratios, depending on the relative density. They predict for aspect ratios lower than 50, that the threshold density value characterizing the transition from zero to n contacts is decreasing with the aspect ratio, but the number of contacts observed at threshold is equal to $n = 8$ independent of the aspect ratio. Flandin et al. proposed in their modeling approach to include the effect of multiple contacts via a reduction factor $N_f/(N_f + N_c)$ affecting the value of the resistance of a network of N_f fibers with total number of contacts N_c [33].

Measurements of conductivity versus frequency reported in the literature show that another power law can be established to describe the frequency dependence of the conductivity, depending on the CNP dispersion state: below or above a percolation threshold. As illustrated in [29] and in Fig. 2.2, below the threshold, corresponding to the lower range of CNP concentrations, the power law describing conductivity versus frequency shows, for each concentration, a linear dependence in double logarithmic scale, over the entire frequency range:

$$\sigma(\omega) \propto \omega^s \tag{2.3}$$

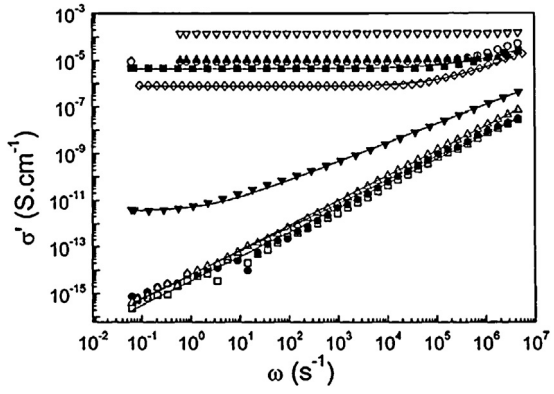

Fig. 2.2. Frequency dependence of electrical conductivity σ' of CNT/epoxy resin composites with weight concentration of 0 (□), 0.04 (●), 0.2 (▲), 0.3 (▼), 0.4 (◇), 0.6 (■), 0.8 (○), 1.5 (▲) and 2.5 wt% (V), from [29]. Solid lines are fits to equation (2.3). Reprinted with permission from [29]. Copyright (2003) American Chemical Society.

Above the threshold, in the upper range of concentrations, the situation is different: the linear behavior is still present in the upper range of the frequency spectrum, while at low frequencies the conductivity shows a nearly constant (or "plateau") behavior versus frequency. The transition frequency between constant and linear behavior is an increasing function of CNP concentration. Also, the percolation threshold can be defined as the CNP concentration where a constant "plateau" behavior starts to appear in the low frequency range of the conductivity-versus-frequency plot.

Observations made for the conductivity can be transposed to the dielectric constant in a reverse manner. The real part of the complex permittivity or dielectric constant (ε'), its imaginary part (ε'') and the corresponding electrical conductivity ($\sigma' = -\omega\varepsilon_0\varepsilon''$) versus frequency curves that are plotted for different CNT loadings (PC nanocomposites) in Fig. 2.3 constitute a very good illustration of the influence of the filler concentration on the electrical properties of nanocomposites, as found in the literature [35]. For low concentrations, below the percolation threshold, the dielectric constant has moderate values that are essentially close to that of the host polymer matrix, which do not vary with frequency. Above the threshold, the dielectric constant exhibits a decrease from high values to low asymptotic values with an inflexion point located at the transition frequency already identified in the frequency dependence of the conductivity.

Power scaling laws are essentially empirical, in the sense that the parameters are fixed from an *a priori* knowledge of the conductivity and dielectric constant behavior, based on experimental observations.

Another family of models aims at describing electrical interactions between CNP inclusions and host matrices, taking

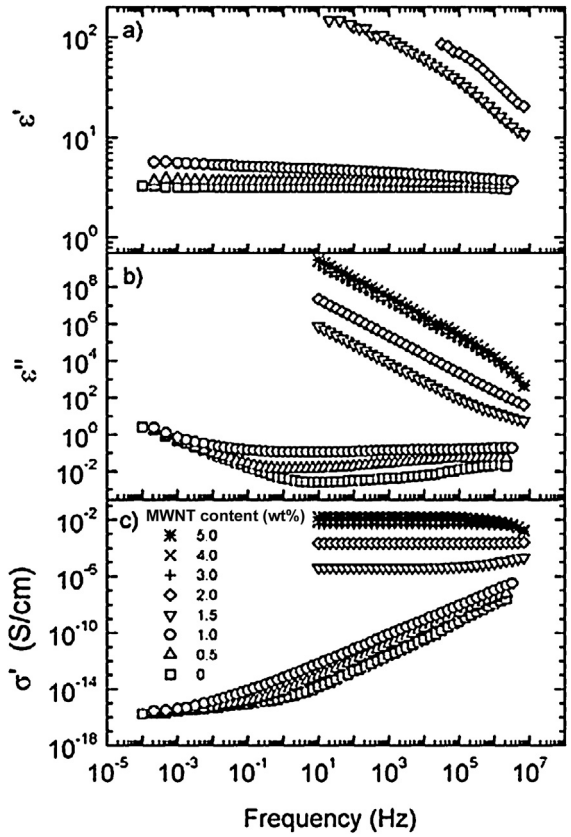

Fig. 2.3. Frequency dependence of the dielectric constant ε' (top), imaginary part of the permittivity ε'' (center) and conductivity σ'' (bottom) of polycarbonate composites with CNT concentrations from 0 to 5 wt%, from [35]. Reprinted from [35]. Copyright (2003), with permission from Elsevier.

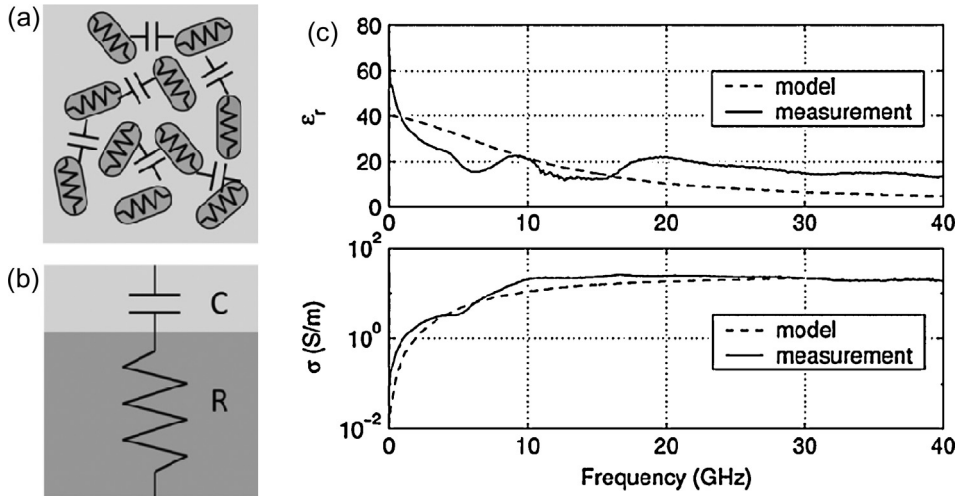

Fig. 2.4. Simple electrical model for the description of the frequency dependence of the conductivity σ' of the nanocomposites: (a) clusters of CNPs, well dispersed inside the polymer foam matrix. CNPs are purely resistive and capacitive couplings between CNPs are shown (b) Equivalent admittance per unit length of the transmission line, superimposed on the equivalent two-layer material (c) Dielectric constant (top) and conductivity (bottom) extracted using the simple electrical model (solid) and from actual measurements (dotted) for a polyethylene (PE) composite with CB content of 50 wt%[44]. Reprinted from [44]. Copyright (2006), with permission from IEEE.

into account their orientation, aspect ratio, interdistance and concentration. The equivalent circuit approach [29,35] illustrated in Fig. 2.4 is a powerful tool for explaining the frequency dependent (or AC) behavior of conductivity and dielectric constant. It models interactions between CNPs and electromagnetic signals by interconnections of resistances and capacitances. The latter, associated to inter-cluster polarization, indeed creates virtual connections at high frequencies between CNPs which explains the increase of conductivity with frequency even when no DC percolation is observable, justifying the concept of "RF percolation": a significant conductivity level of the nanocomposite is reached at radio and microwave frequencies, while no DC percolation occurs, due to the lack of physical interconnected network of CNPs. Several models have been proposed for calculating R and C components of the equivalent circuit. Again the pioneering work of Kirkpatrick [32] must be acknowledged as one of the first modeling approach for the equivalent conductance $G = 1/R$ of randomly connected resistor networks, enabling to take into account percolation threshold effects. Later, numerical approaches have been improved in order to predict the full AC response. Most of these approaches include a capacitance C for modeling either the inter-cluster polarization or diffusion within conductive clusters. In particular, Clerc et al. expanded the approach of Kirpatrick by considering network of electrical impedances (R-C elementary cells) that are randomly connected or not, with R or C randomly removed or not in each cell [43].

A last powerful modeling approach is based on the effective medium theory (EMT). Using EM field averaging techniques, the values of the macroscopic effective permittivity of the real heterogeneous medium, or equivalently its dielectric constant and conductivity can be predicted over the entire frequency range as a function of the concentration of inclusions, orientation (randomly dispersed or aligned along a particular direction) and shape aspect ratio (sphere, wire or platelet). A review of EMTs is provided in the book of Ari Sihvola [45], including the popular Bruggeman EMT and the Maxwell-Garnet approximation. The latter considers that the effective permittivity for a mixture of spherical inclusions (ε_i) in a host external medium (ε_e) having volumetric fraction f of inclusions (Fig. 2.5b and c) can be derived from a « volumetric » averaging or homogeneisation procedure, yielding:

$$\varepsilon_{\text{eff}} = \varepsilon_e + 3f\varepsilon_e \frac{\varepsilon_i - \varepsilon_e}{\varepsilon_i + 2\varepsilon_e - f(\varepsilon_i - \varepsilon_e)} \tag{2.4}$$

The Maxwell-Garnet formulation is applicable to lossy inclusions and host material, i.e. having their complex permittivity (or permeability), and is a function of the dielectric constant ε' and conductivity σ. It can be easily extended to inclusions with shape anisotropy that are modeled as ellipsoids, oriented or randomly dispersed in the host (Fig. 2.5). The nanotubes are handled as cylinders considered as a limit case of the ellipsoidal shape. Finally, the formulation is also valid for effective permeability associated to magnetic inclusions, simply obtained by replacing permittivity of the matrix and of the inclusions by their respective permeability [45].

2.2. Modeling of wave propagation in CNP composites

Propagation of electromagnetic waves through a slab of composite material described by scalar parameters ε, μ and having a thickness t is described via a transmission line formalism associated to electric (E) and magnetic (H) field components. Assuming normal incidence of the wave with respect to the air-

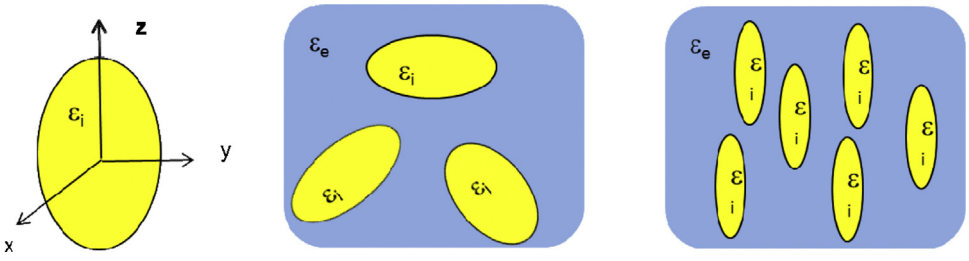

Fig. 2.5. (a) Generalized ellipsoid representation of nanoinclusions, having (b) random, or (c) aligned, orientation.

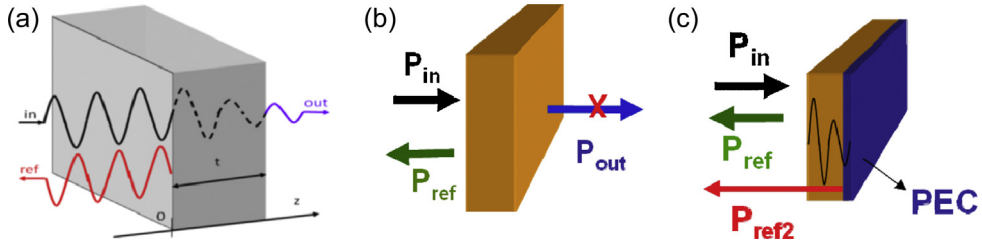

Fig. 2.6. EMI shielding concepts for a slab of conductive nanocomposite (a) wave propagation and reflection (b) definition of incoming, reflected and transmitted power for shielding effectiveness SE (c) configuration for definition of reflectivity *R*.

material interface, the field components have the following *z*-dependence in each of the 3 areas, see Fig. 2.6a.

$$\text{Input air region } z<0: \quad E = V_{+a1}e^{-\gamma_a z} + V_{-a1}e^{\gamma_a z}$$
$$H = Y_a(V_{+a1}e^{-\gamma_a z} - V_{-a1}e^{\gamma_a z}) \tag{2.5}$$

$$\text{Composite}: 0<z<t: \quad E = V_{+c}e^{-\gamma_c z} + V_{-c}e^{\gamma_c z}$$
$$H = Y_c(V_{+c}e^{-\gamma_c z} - V_{-c}e^{\gamma_c z}) \tag{2.6}$$

$$\text{Output air region } z>t: \quad E = V_{+a2}e^{-\gamma_a (z-t)}$$
$$H = Y_a V_{+a2}e^{-\gamma_a (z-t)} \tag{2.7}$$

with, for air, the complex propagation constant $\gamma_a = j\omega/c_o$, the angular pulsation $\omega = 2\pi f$, the frequency f, the velocity of light c_o, and the wave admittance $Y_a = \gamma_a/j\omega\mu_o$, and, for the composite, the complex propagation constant $\gamma_c = j\sqrt{\varepsilon_r\mu_r}\omega/c_o$, and the wave admittance $Y_c = \gamma_c/j\omega\mu_o\mu_r$. In the latter expressions, complex permittivities and permeabilities can be calculated using any of the formalisms proposed in Section 2.1. Indeed, the knowledge of the influence of the conductive filler content on conductivity and of the dielectric constant (via power laws, RC equivalent circuit or effective medium theory) enables to calculate the complex value of γ_c, which is the key parameter involved in the modeling of the reflection and absorption of power, hence on the SE performances, as will be shown in this section.

Forward terms with a subscript "+" represent a wave propagating along positive *z*-axis, while terms with a subscript "−" hold for a wave propagating in the reverse direction. This transmission line formalism using complex phasors ensures that all successive reflections occurring in the time domain at input ($z = 0$) and output ($z = t$) air-slab interfaces are taken into account. It is thus more general than the approximate analytical formulations proposed in the literature for the shielding effectiveness, that usually do not take into account such multiple reflections. Imposing the continuity of E and H fields on input and output air-slab interface (at $z = 0$ and t respectively) yields an efficient matrix formulation of the problem, relating electric and magnetic field at the input interface, denoted by subscript 'in', to the corresponding at the output interface, denoted by subscript 'out'.

$$\begin{bmatrix} E_{in} \\ H_{in} \end{bmatrix} = \begin{bmatrix} A & B \\ C & D \end{bmatrix} \begin{bmatrix} E_{out} \\ H_{out} \end{bmatrix} = \begin{bmatrix} \cosh\gamma_c t & Z_c \sinh\gamma_c t \\ Y_c \sinh\gamma_c t & \cosh\gamma_c t \end{bmatrix} \begin{bmatrix} E_{out} \\ H_{out} \end{bmatrix} = [T_c] \begin{bmatrix} E_{out} \\ H_{out} \end{bmatrix} \tag{2.8}$$

The so-called transfer or chain matrix, noted $[T_c]$, is particularly useful for further modeling of multilayered structures, since the global transfer matrix of a stack of n layers is simply obtained by the matrix product of the corresponding matrices:

$$T_{tot} = \prod_{i=1}^{n} T_{c_i} \tag{2.9}$$

A variant but equivalent formulation for multilayered structures is provided in [46].

On the other hand, the power absorbed in the composite slab is obtained from the power balance between the power respectively incident in the air region 1 (P_{in}), the power reflected at input interface air/composite (P_{ref}), and the power transmitted into region 3 (P_{out}):

$$P_{abs} = P_{in} - P_{ref} - P_{out} \tag{2.10}$$

From a microwave point of view, modern instrumentation using scalar [47,48] or Vector Network Analyzer [49] (VNA) coupled with either coaxial [50] or rectangular waveguide sample holders/launchers [46,51–53] allows the simultaneous measurement of the reflected and transmitted power at the two ports over a given frequency range. It measures the scattering parameters S_{ij} (or *S*-parameters), phase and magnitude, that are characteristic of the device connected between the two ports: $|S_{11}|^2 = P_{ref}/P_{in}$ corresponds to the power reflected back at port 1, normalized to the incoming source power P_{in}, while $|S_{21}|^2 = P_{out}/P_{in}$ is related to the power transmitted from port 1 to port 2, through the device, also normalized by the incoming power P_{in}. The ratio of the power absorbed by the sample (P_{abs}) to source power can be thus expressed by virtue of (2.10) as

$$A = \frac{P_{abs}}{P_{in}} = 1 - |S_{11}|^2 - |S_{21}|^2. \tag{2.11}$$

Straightforward analytical formulas convert chain matrix components to corresponding *S*-matrix components:

$$S_{11} = \frac{Z_a A + B - Z_a^2 C - Z_a D}{Z_a A + B + Z_a^2 C + Z_a D}$$
$$S_{21} = \frac{2Z_a(AD - BC)}{Z_a A + B + Z_a^2 C + Z_a D} \tag{2.12}$$

For a monolayer composite slab, represented by a single chain matrix T_c (2.8), simple expressions are derived using (2.12) for the various terms involved in (2.10–2.11):

$$\frac{P_{ref}}{P_{in}} = |S_{11}|^2 = \left|\frac{\Gamma\left(T^2 - 1\right)}{1 - \Gamma^2 T^2}\right|^2$$
$$\frac{P_{ref}}{P_{in}} = |S_{21}|^2 = \left|\frac{T^2(1 - \Gamma)}{1 - \Gamma^2 T^2}\right|^2 \tag{2.13}$$

where Γ is the interfacial reflection coefficient

$$\Gamma^{\Delta} = \frac{Y_c - Y_a}{Y_c + Y_a} = \frac{\sqrt{\varepsilon_r/\mu_r} - 1}{\varepsilon_r/\mu_r + 1} \tag{2.14}$$

while T is the transmission coefficient of the wave over thickness t of the slab:

$$T^{\Delta} = e^{-\gamma_c t} \tag{2.15}$$

Two more parameters are of prime interest for the evaluation of the EMI shielding performances. The shielding effectiveness noted

SE quantifies the ability of the slab to stop the transmission of the signal, and is simply obtained as the inverse of the normalized transmitted power:

$$SE = \frac{P_{in}}{P_{out}} = \frac{1}{|S_{21}|^2} = \left|\frac{1-\Gamma^2T^2}{T\left(1-\Gamma^2\right)}\right| \tag{2.16}$$

The reflection R at the input of the sample expresses similarly as:

$$R = \frac{P_{ref}}{P_{in}} = |S_{11}|^2 = \left|\frac{\Gamma\left(T^2-1\right)^2}{1-\Gamma^2T^2}\right| \tag{2.17}$$

and quantifies the ability of the slab to reflect waves incoming at the input interface. A variant of this definition is the reflectivity R', measuring or computing the ratio of the reflected to the incoming wave at the input interface when the output interface is backed by a perfect metallic plane [54] that ensures a total reflection of waves back to the input interface. It is expresses as

$$R' = \left|S_{11} + \frac{S_{21}^2}{1+S_{11}}\right|^2 = \left|\frac{Z_c\sinh\gamma_c t - Z_a\cosh\gamma_c t}{Z_c\sinh\gamma_c t + Z_a\cosh\gamma_c t}\right|^2 \tag{2.18}$$

A low reflectivity will thus ensure simultaneously that reflection at the input interface 1 ($R = |S_{11}|^2$) is minimized and that the power A absorbed inside the slab is maximized. Other said, the slab acts as an efficient wave absorber or Radar Cross Section (RCS) reducer. Concepts of reflection, transmission and reflectivity are summarized in Fig. 2.6.

Expression (2.16) reveals that the shielding effectiveness SE is maximized if the magnitude of the transmission factor T is minimized, meaning that the real part of the complex propagation constant $\gamma_c = j\sqrt{\varepsilon_{eff}}\omega.c_o$ is maximized. This also means that for nonmagnetic composites ($\mu_r = 1$) the imaginary part of permittivity $\varepsilon_{eff} = \varepsilon_r - j\sigma/\omega\varepsilon$ has to be maximized, hence that the conductivity of nanocomposites has to be maximized. The minimization of T resulting from maximization of conductivity also means that most of the entering power is dissipated inside the composite, with, as a result, the minimization of the transmitted power.

Similarly, the reflection R will be minimized if the input interfacial reflection coefficient Γ (2.14) is minimized, implying that the (effective) dielectric constant ε_r of the composite material has to be kept close to one.

It must be emphasized that the right-hand sides of expressions (2.16) to (2.17) are particular cases valid only for a single slab. For multilayered structures, only the general definition involving S-parameters is applicable, i.e. using expressions (2.12) written with the elements of the global chain matrix T_{tot} of the stack, given by (2.9).

Expression (2.11) can be rewritten as the sum of two terms as well

$$SE = 10\log_{10}\left|\frac{1}{|S_{21}|^2}\right| = 10\log_{10}\frac{1}{1-|S_{11}|^2} + 10\log_{10}\frac{1-|S_{11}|^2}{|S_{21}|^2} = SE_R + SE_A \tag{2.19}$$

Which is very often presented in the literature [47,48,51] as a convenient way to estimate separately the contribution of reflection and absorption to the global shielding of a slab material. Also, the transmission factor T, when expressed in dB, is often associated to the (partial) shielding effectiveness by absorption via the relationship $SE_A = 20\log 10T$ approximating the contribution to the global shielding of attenuation/absorption inside the slab (or equivalently of the power dissipated inside the slab) [47,48]. This is only true when multiple reflections at the input and output interfaces can be neglected. Otherwise, only expression (2.11) using S-parameters (2.12) is applicable [48] for the total power absorption.

As a first design rule, an efficient microwave absorber must combine a low reflection of waves at the interfaces with surrounding air, and a good absorption obtained by conductive dissipation of the entering power over the slab thickness. However, this requires simultaneously a low dielectric constant (as close as possible to air) and a high conductivity (close to 1 S/m), respectively. These two requirements are antagonist, as was already shown in Section 2.1, since an increase in conductivity induced by a higher CNP loading goes in hand with an increase of the dielectric constant. This issue can be solved for a given slab thickness by replacing a single layer of nanocomposite by a multilayer of similar overall thickness with successive layers showing increasing CNP concentration [28,55]. Hence, a moderate increase of the dielectric constant and of the conductivity is created, preventing reflection at the input interface while preserving sufficient progressive conductive dissipation over the slab thickness. The chain matrix product (2.9) is thus particularly relevant to model such multilayered structures, since each layer is described by its own chain matrix having parameters γ_{ci} and Z_{ci} taking into account its own CNP concentration.

3. Polymer/carbon based composites as EMI shielding materials

3.1. Graphite and carbon black as conductive fillers

Carbon black (CB) is the accepted generic name for a family of small particle size carbon pigments which are formed in the gas phase by thermal decomposition of hydrocarbons [56]. It represents the predominant reinforcing filler used in rubber compounds thanks to their beneficial impact on durability and strength. Carbon blacks do not exist as primary particles and are generally fused into aggregates. The shape and degree of aggregate branching is referred to as starting structure. Increasing structure typically increases modulus, hardness, electrical conductivity and compound viscosity and improves dispersability of carbon black.

Rubber (EPDM [57], SBR [58], ethylene acrylic [59], siloxane [60]) and rubber based blends (EVA/NBR [61], NR/BR [62], BR/LDPE [63]), are the most common matrices envisioned for the preparation of carbon black filled EMI shielding materials. The general method to prepare these composites is by melt mixing (in a roll-mill or in an internal mixer) followed by a curing step at a temperature that depends on the material. The performances of SBR/CB composites are relatively poor since a large CB content (35 wt%, 8–12 GHz, t = 0.65 cm) or a large thickness (15.3 wt%, 8–12 GHz, t = 7 cm) is necessary to achieve a shielding effectiveness of 20 dB [58]. The EPDM/CB composites develop higher SE after vulcanization but, again, a very large CB loading is necessary to achieve 20 dB (35 wt%, 8–12 GHz, t = 5.5 mm) [57]. Interestingly, a treatment at high temperature (175 °C) improves the electrical conductivity by increasing the contact between CB particles. The study on EVA/NBR/CB composites highlighted the importance of the degree of contact between CB particles on the electrical conductivity and, consequently, on EMI shielding properties [61]. First, the SE increases with the NBR content in the blends thanks to a more uniform distribution of CB and improved CB-CB contacts. Secondly, the comparison between two kinds of CB shows that the shielding effectiveness is much higher for the CB having higher starting structure (the starting degree of aggregation of CB particles). The preservation of contacts between the particles during the melt-mixing is more probable in this case. Relatively large filler loading (25 vol%) was also necessary to achieve a SE of 20 dB (0.5–5 GHz) in NR/BR 70/30 blends but the measurement

was performed on samples with a small thickness (2 mm) [62]. The addition of 7 wt% LDPE within SBR was improving the conductivity and the SE of the 17 wt% CB filled composites [63]. At this concentration, LDPE form fiber like structure that helps the formation of a percolating CB network. At higher LDPE content, the conductivity and SE tends to decrease.

CB particles have also been dispersed within thermoplastic (LLDPE [64], chlorinated polyethylene [65], polypropylene [66]), resin (epoxy [67,68]) and blends of thermoplastic polymer (PS and PP) [69]. In the latter study, the conductivity and, consequently, the SE is higher in PP compared to PS because, first, the filler is ejected from the crystalline phase of PP (and then concentrated in the amorphous phase) which decreases the average distance between CB particles and, second, the higher surface tension between CB and PP favors the agglomeration of the CB particles leading to a more efficient conductive network. The SE of the blends filled with 10% vol CB lies between the one of the pure matrices and is around 17 dB (0.1–1 GHz) at a thickness of 2 mm.

3.2. Carbon fibers as conductive fillers

Originally, carbon fibers were manufactured by graphitization of PAN or petroleum pitch but the more affordable vapor grown process from hydrocarbon has become the most important preparation technique [70,71]. The morphology, structure and dimension greatly depend on the catalyst and the source of carbon. Nickel, copper, iron and their alloys are the main catalysts used while the sources of carbon generally involve propane, ethylene and acetylene [70]. The morphology of these vapor grown carbon nanofibers (VGCNF) can be linear, helical or twisted. Their diameter generally lies between 50 and 200 nm and the length can be superior to 50 μm giving rise to aspect ratios around 250 and 2000.

3.2.1. Melt-mixing CNF

Das et al. were very active at the beginning of the years 2000s in the preparation of carbon nanofibers composites for EMI shielding [72–75]. The attention was focused on EVA matrix which gives better performances compared to EPDM and to natural rubber thanks to its higher polarity. For example, 8 wt% of CNF are needed to reach 20 dB in the EVA composites while this level is only reached at 17.5 wt% with the NR composites (12 GHz, t = 3.5 mm) [72]. The performances of the EPDM composites are closer to the EVA ones but still in the advantages of the polar matrix [74,75]. However, a major improvement of the SE was observed when these two matrices were blended in equal quantity (50/50). Thanks to the exclusive localization of the CNF within one phase and consequently to a lower average distance between carbon particles, the SE reaches 40 dB (8–12 GHz, t = 3.5 mm) at 9 wt% of CNF compared to 20 dB for the EVA composite [74,75]. Throughout their studies, the authors compared the efficiency of the CNF with CB particles. Whatever the matrix, the SE measured was much higher for the nanofiber owing to their aspect ratio which favors contact between particles. For instance, a content of 33 wt% of CB in EVA is needed to reach a SE of 20 dB compared to 9 wt% of CNF (12 GHz, t = 3.5 mm).

The advantage of the high aspect ratio of CNF is confirmed by the study of Jana et al. on CNF/polychloroprene rubber composites [76,77]. Two different mixing techniques, i.e. roll-mill method and cement mixed method, have been compared. The second method, which consists in pre-dispersing the polymer and the CNF within a solvent before roll-milling during a much shorter time than for the first method, is less aggressive for the CNF hence preserving a higher aspect ratio (100 vs. 25). Consequently, the measured SE was much higher (20 dB vs. 10 dB at 1 GHz, t = 1.7 mm). The comparison between the SE of short (l = 1 mm) and long (l = 5 mm) carbon fibers dispersed in Nylon-66 composites is also in favor of the higher aspect ratio of the filler (40 dB vs. 20 dB, filler content 20 wt%, 1.5 GHz, t = 1.2 mm) [50]. Nylon composites were also used to compare the SE of carbon black, synthetic graphite with an aspect ratio of 1.8 and carbon fibers with an aspect ratio around 80 [52,78–80]. In contrast to the previous studies, carbon black was here the most efficient filler (20 dB at 7 wt%, 800 MHz) followed by the carbon fiber (14 dB at 25 wt%, 800 MHz) and the synthetic graphite (12 dB at 25 wt%, 800 MHz) [80]. The authors do not explain this strange behavior but a lower quality of dispersion for the carbon fiber and the synthetic graphite could possibly account for these observations. A combination of these three fillers leads to synergistic effect [80].

SE superior to 20 dB was also reached by dispersing 5 wt% vapor grown carbon fibers within chlorobutyl rubber by roll-mill (8–10 GHz, t = 1.014 cm) [81] while 30 dB was reached with only 3 wt% of CNF within polysulfone (8–12 GHz, t = 1 mm) [82].

During their study on HDPE/VGCNF composites, Al-Saleh et al. determined the effect of mixing speed, time and temperature on the properties of the resulting materials [83,84]. The two first parameters tend, when increased, to improve the quality of the dispersion however at the expense of the VGCNF aspect ratio. Consequently, the resulting SE decreases when the mixing time and speed increase (Fig. 3.1a). In contrast, when the temperature increases, the shearing rate during melt-mixing decreases, inducing a dispersion of lower quality and a better conservation of the nanofiber aspect ratio. However, in this case, the improved aspect ratio does not compensate the decrease in quality of the

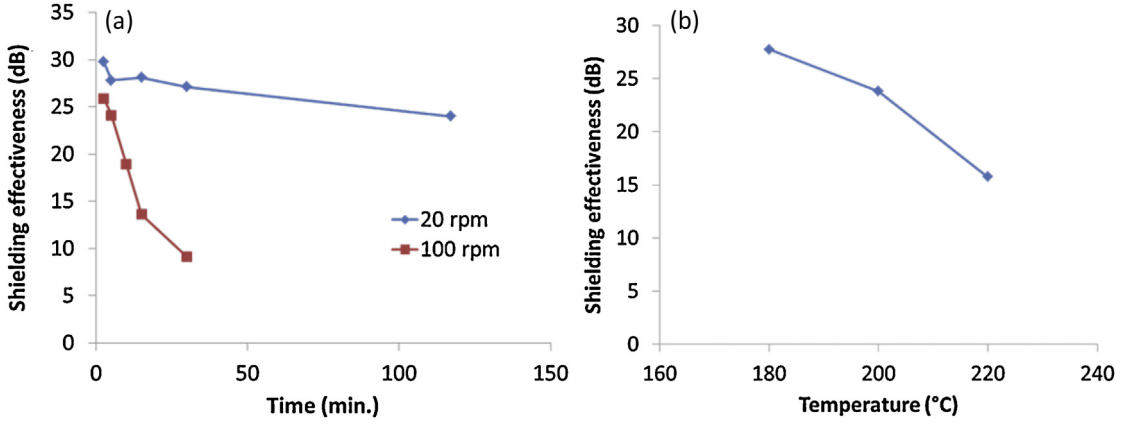

Fig. 3.1. (a) EMI SE of 7.5 vol% VGCNF/HDPE composites at 1 GHz and at different processing condition (20 rpm and 100 rpm) as a function of time; (b) EMI SE of 7.5 vol% VGCNF/HDPE composites processed at 50 rpm as a function of the processing temperature [84].

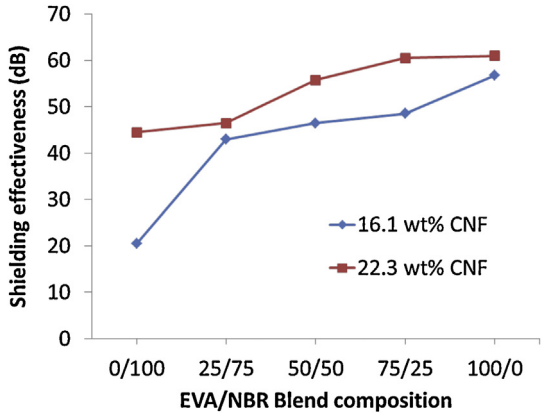

Fig. 3.2. Variation of the EMI SE of EVA/NBR/CNF blends as a function of the blend composition at 10 GHz (t = 5 mm) [85].

dispersion and the SE decreases with the mixing temperature (Fig. 3.1b). This study highlights the importance of an appropriate CNF dispersion to achieve optimum shielding efficiencies. Indeed, the CNF must be disaggregated enough to establish a conductive network but the shearing rate to achieve this target must not be too high to preserve a high CNF aspect ratio and enough contact between carbon particles.

Such as for carbon black, carbon fibers have been dispersed within EVA/NBR blends. Meanwhile, the conductivity and SE decrease with the content of NBR as a result of a higher amount of CNF cutting (10 GHz, t = 5 mm) (Fig. 3.2) [85].

Jou et al. have used a liquid crystalline polymer based on aromatic polyester to induce a preferential CNF orientation in an injection molding [86] process. An increase from 30 dB to 50 dB (20% CNF, 1 GHz, t = 3 mm) compared to a more random orientation has been observed when the measurement is performed with the electrical field oriented parallel to CNF.

3.2.2. Other dispersion methods

Solution coating was also investigated for the preparation of EMI shielding materials based on PVDF [87,88] and PVOH [89]. After an ultrasonic treatment, the solvent of the polymer/CNFs solution is evaporated to form nanocomposite films. In order to compare the SE of carbon fillers with different morphologies and physical properties, Lee et al. prepared several CNF from different precursor gas type (propane, ethylene and acetylene) and various catalyst compositions (nickel-copper and pure nickel) [89]. The morphology of carbon nanofibers was sensitive to the type of hydrocarbon gas. The carbon nanofibers prepared from propane consisted mostly of linear conformation and those from ethylene exhibited essentially a twisted conformations. The carbon nanofibers from acetylene had both twisted and helical conformation. The electrical conductivity and consequently the SE of the PVOH composites were not proportional to the conductive properties of the nanofillers but more sensitive to the specific surface area which confirms again the importance of an optimum contact between the carbon particles in order to achieve high EMI shielding properties [89]. The best EMI SE were obtained with the carbon fiber prepared starting from ethylene and Ni-Cu catalyst and was around 5 dB (1 GHz, t = 30 μm). Finally, carbon nanofibers were also dispersed before the curing of epoxy resins in order to improve their complex permittivity and consequently their shielding properties [90–93]. The shielding effectiveness has been improved by activation of the CNF, i.e. through an increase of the specific surface area by formation of pores at their surface by chemical and heat treatment [90,91]. Since the reflection of these composites remains constant after the activation, the improvement of the SE is due to other shielding mechanisms, i.e. absorption and/or to multi-reflection [90]. In order to improve the efficiency of CNFs, Singh et al. have grown carbon nanotubes on their surface [94]. The shielding effectiveness of samples with a total carbon filler content of 30 wt% is accordingly improved from 19 to 38 dB when the CNTs amount is raised up to 3 wt% (10 GHz, t = 2.5 mm).

3.3. Carbon nanotubes as conductive fillers

Carbon nanotubes can be considered as rolled-up hollow cylinders of graphene sheets. They can be constituted of a single hollow cylinder, i.e. single-walled carbon nanotubes (SWNTs) or of a collection of graphene concentric cylinders, i.e. multi-walled carbon nanotubes (MWNTs). Three methods are mainly used for the synthesis of CNTs: electric arc discharge [95–98], laser ablation [99–101] and chemical vapor deposition [102,103]. Due to their very small diameter, CNTs possess a very high aspect ratio. They therefore offer substantial advantages over conventional carbon fillers because, if properly dispersed, percolation occurs at very low contents (<2 wt.%).

3.3.1. Melt-mixing CNT

When EMI shielding applications are envisioned, melt-mixing is the main dispersion method used for the preparation of CNTs composites based on poly(trimethylene terephthalate) (PMTT) [104–106], poly(ethylene terephthalate) (PET) [107], poly(ethylene) (PE) [107,108], polycarbonate (PC) [109,110], poly(propylene) (PP) [47,107,111,112], poly(ethylene-vinyl acetate) (EVA) [113], poly(ethylene methyl acrylate) (EMA) [114,115], poly(ether ether ketone) (PEEK) [116], acrylonitrile-butadiene-styrene copolymer (ABS) [117], poly(caprolactone) (PCL) [118] and poly(L-lactide) (PLLA) [119]. The direct dispersion of CNTs within PMTT leads to SE superior to 20 dB at only 5 wt% (12–18 GHz, t = 2 mm) with a shielding mechanism mainly based on absorption [104–106]. The masterbatch method that consists in the dilution within the main polymer matrix of carbon nanotubes pre-dispersed at a high loading in a polymer, has been used for the preparation of PP and PC nanocomposites [47,109]. This method favors the dispersion of the CNTs and limits, during the dispersion step, the volatilization of the nanotubes. By this way, SE higher than 15 dB has been achieved at 7 wt% of CNTs within PC (0.1–1.6 GHz, ASTM D4935-90). Still in PC nanocomposites, Arjmand et al. have studied the influence of CNTs orientation on EMI properties by comparing samples prepared by compression and injection molding [110]. Due to the high shear during the injection process, CNTs preferably orient parallel to the flow. The electrical conductivity appeared to be lower in the oriented samples whatever the direction of measurement most probably due to a lower amount of direct CNT-CNT contacts. These conclusions have been confirmed on a similar study carried out on PS nanocomposites [120,121]. While melt-mixing is by far the first choice for industrial production of nanocomposites, it however suffers from an intensive break-up of the CNTs, as it was the case for carbon nanofibers, significantly reducing their aspect ratio. The electrical conductivity and, consequently, the shielding effectiveness are then negatively affected as demonstrated for PCL nanocomposites [44,118]. A comparison between melt-mixing and co-precipitation reveals that while the length of the CNTs is preserved with the second method (l > 1 μm), a large reduction of length is observed when melt extrusion is concerned (l < 500 nm). This decrease is even more pronounced when CNTs with higher structural defects are used (l < 200 nm). The electrical conductivity of the nanocomposites prepared by co-precipitation is then much higher, therefore resulting in SE superior to 25 dB at very low CNTs content (0.7 wt%, 25–40 GHz, t = 3 cm). In this study, melt-mixing of CNTs in different matrices (PCL, PS, PEtOc, PVC, PMMA, PC, PP) was also

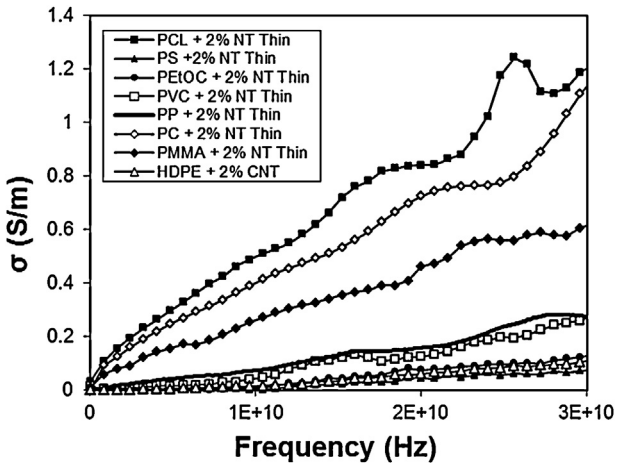

Fig. 3.3. Variation of the electrical conductivity σ' as a function of frequency for PCL, PS, poly(ethylene-co-octene), PVC, PMMA, PC and PP filled with 2 wt% of CNT [118]. Reprinted with permission from [118]. Copyright (2007) American Chemical Society.

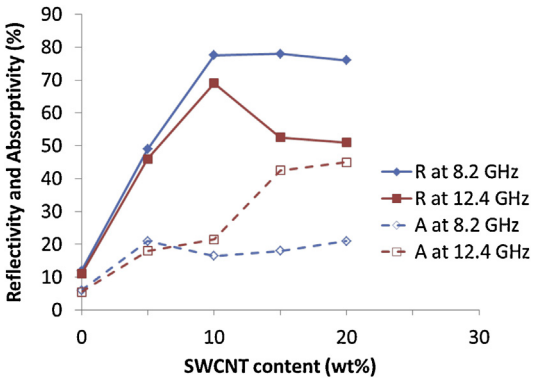

Fig. 3.4. reflectivity (R) and absorptivity (A) vs. SWNT loading at different frequencies of PUR/SWNTs nanocomposites prepared by solvent casting [51].

compared and only the polymers possessing a carbonyl group in their constitutive monomer (PCL, PMMA, PC) involved significant electrical conductivity (>1 S/m) owing to a better CNTs dispersion (Fig. 3.3). It was suggested that π-π interactions between the aromatic structure of the nanotubes and the carbonyl groups in the chains are very beneficial to the morphology of the nanocomposites and to their electrical properties. The negative effect of CNTs break-up during melt-mixing was also highlighted with EVA nanocomposites for which lower SE were obtained compared to solution mixing (6 dB vs. 4 dB at 9 wt%, 8–12 GHz) [122].

In order to improve their dispersion within poly(L-lactide) (PLLA), CNTs have been modified by polyhedral oligomeric silsesquioxanes (POSSs) via amidation reactions [119]. As a consequence, the PLLA/MWCNT-g-POSS composites showed better EMI shielding than PLLA/MWCNT composites (15 dB vs. 11 dB at 4 wt% and 40 GHz, ASTM D4935-99).

The poor quality of the dispersion is a major limitation for the production of CNTs polypropylene composites [123–125]. New compatibilizers have thus been prepared by reactions of aminomethylpyridine and of an amino-pyrene derivative with commercially available polypropylene-graft-maleic anhydride in the melt [112]. These small molecules adsorb on the CNTs surface via π-π interactions. The co-precipitation and melt-blending techniques were used to disperse the nanofillers within the compatibilizers, before dispersion in PP by melt-blending. The co-precipitation appeared to be the most efficient technique probably because it allows the application of an ultrasonic treatment. In contrast to unmodified PP-g-MA, the two compatibilizers were able to significantly increase the conductivity of PP/CNTs nanocomposites. The best results were obtained when using polypropylene grafted by aminomethylpyridine as the CNTs compatibilizer. The SE was then improved to 30 dB (2 wt%, 30 GHz, t = 3 cm) compared to 10 dB without compatibilizer.

3.3.2. Other dispersion methods

Solvent casting is another widely used dispersion technique for the preparation of polymers CNTs nanocomposites devoted to EMI shielding. It was used for PC [126], PMMA [127], PS [127], PUR [128,129], PVDF [130], PVP [130], LDPE [131], cellulose triacetate [132] and lotader epoxy [133,134]. It consists in the solubilization of the polymer in a CNTs based solution followed by the evaporation of the solvent. For the PC nanocomposites, an H_2O_2 treatment on the CNTs significantly reduces the percolation threshold from 3 wt% to 0.5 wt% thanks to a better dispersion [126]. The SE is then significantly improved from 4 dB to 11 dB at 5 wt% (1–12 GHz, ASTM D4935-99). Mathur et al. have compared the performances of PS and PMMA nanocomposites prepared by solvent casting and obtained similar shielding effectiveness (18 dB at 10 vol%; 8–12 GHz, t = 0.3 mm) which was directly related to the electrical conductivity of the samples [127]. The solvent casting method was also used to disperse SWNTs within PUR. The addition of the nanofillers increases the SE to 18 dB at 20 wt% (8–12 GHz, t = 2 mm). Reflection is the main shielding mechanism but the relative contribution of absorption increases with the filler content (Fig. 3.4). The electrical conductivity of CNTs composites based on PVDF/PVP blends was much higher than the respective homopolymer composites leading to interesting SE levels (20 dB at 0.4 wt%, 0.1–1.5 GHz, ASTM D4935) [130]. The MWNTs were synthesized in laboratory by the catalytic decomposition of a ferrocene-xylene mixture. A heat treatment at 1100 °C on the MWNTs before their dispersion adversely affects the SE although a better intrinsic conductivity of the nanofillers was measured. A decrease in the specific surface area is the obvious origin for this observation. The difficulty to impart electrical conductivity to LDPE was overcome by the use of laboratory synthesized MWNTs with very high aspect ratio (diameter = 10–70 nm, length > 200 μm) [131]. Solvent casting was preferred over melt-mixing in order to preserve the high aspect ratio of the nanofillers. A 20 dB SE was reached at 10 wt% (12–18 GHz, t = 1.65 mm). Park et al. have used carboxylic acid functionalized SWNTs to form a chemical bond with the polymer matrix by reaction with the epoxide group of a reactive ethylene terpolymer [133]. Even though the functionalization of single-walled carbon nanotubes disrupts the electronic structure and consequently damages the conductive properties, the more uniform dispersion compared to unfunctionalized SWNTs improves more efficiently the real and imaginary part of the permittivity which is beneficiary for shielding properties. The enhancement was also larger than in the case of MWNTs functionalized by carboxylic acid groups that are characterized by a lower aspect ratio.

Several studies have also been devoted to the preparation of cured resin (epoxy [135–143], melamine formaldehyde [144])/CNTs nanocomposites. Huang et al. have compared the SE of composites based on three different SWNTs that varied by their aspect ratio and/or wall integrity [137,138]. The filler with the highest aspect ratio is again the most efficient to impart shielding properties to the materials thanks to a lower percolation threshold. The improvement of the wall integrity by annealing the SWNTs at 1100 °C also increases the shielding effectiveness of the composites. A 20 dB SE was then achieved with 15 wt% of "long SWNTs" and "annealed-short SWNTs" (8–12 GHz, t = 2 mm). Im et al. improved the compatibility between epoxy resin and MWNT by increasing the hydrophobicity of the nanofillers via a fluorination

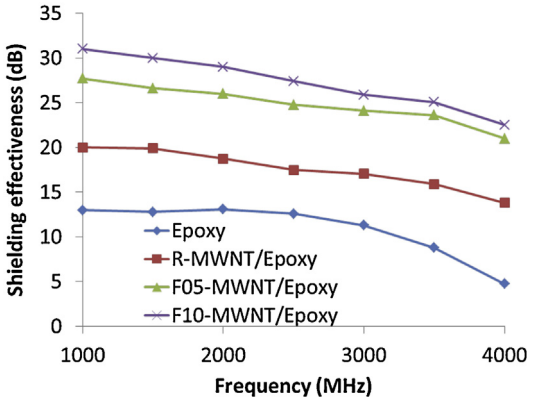

Fig. 3.5. EMI SE as a function of frequency of epoxy resin filled with raw MWNTs (R-MWNT) and MWNTs treated with fluorine gas at a pressure of 0.5 bar (F05-MWNT) and 1 bar (F10-MWNT [135]).

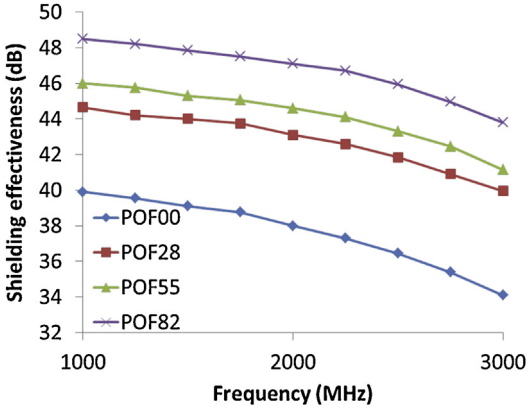

Fig. 3.7. EMI SE of polyaniline filled with 1 wt% of raw MWNTs (POF00) and MWNTs treated with different mixture of O_2/F_2: 8/2 (POF82), 5/5 (POF55) and 2/8 (POF28) [145].

treatment [135]. A better CNTs dispersion and consequently a better shielding effectiveness were achieved (30 dB vs. 20 dB for raw CNTs at 2 GHz, ASTM D-4935-99) (Fig. 3.5).

Several carbon fillers were also compared within melamine formaldehyde resin [144]. The better efficiency of the carbon nanotubes compared to amorphous carbon and graphite was confirmed. During this study, CNTs were also dispersed with a liquid crystal polymer matrix able to orient the CNTs. A better shielding efficiency was obtained which could be attributed to the orientation. However, since it is not the only parameter that changes between these composites, attention should be made before drawing a final conclusion.

Another technique widely used for the processing of nanocomposites is the in situ polymerization which consists in polymerizing a monomer in the presence of the nanofillers. This technique was mainly used for the preparation of polyaniline (PANI) nanocomposites [48,145,146]. When doped, this polymer is electrically conductive and can already shield the electromagnetic radiation. CNTs are added to improve the shielding effectiveness by reflection and absorption (Fig. 3.6) [48]. The absorption is significantly improved by increasing the CNTs content, and becomes the dominant shielding mechanism. The introduction of polar groups by oxyfluorination of CNTs improves their dispersion within PANI [145]. The SE appeared to be improved with this treatment especially as the O_2/F_2 ratio increases (Fig. 3.7).

PMMA nanocomposites were also prepared by in situ polymerization of MMA in the presence of CNTs in a dimethylacetamide solution [147,148]. The material is then recovered by removing the solvent at 120 °C for 72 h. The resulting SE was higher compared to nanocomposites prepared by solvent casting (15 dB vs. 10 dB at 4.76 wt%, 2–18 GHz) [147]. Alternatively, the coagulation (or coprecipitation) technique was also envisioned to prepare PMMA/SWNTs [149], PCL/MWNTs [44,118] and PS/MWNTs [150] nanocomposites. This method consists in solubilizing the polymer in a CNTs solution and co-precipitating the two components in a poor solvent of the polymer. By this technique, 20 dB SE was obtained at 8 wt% of SWNTs (8–12 GHz, t = 4.5 mm) [149].

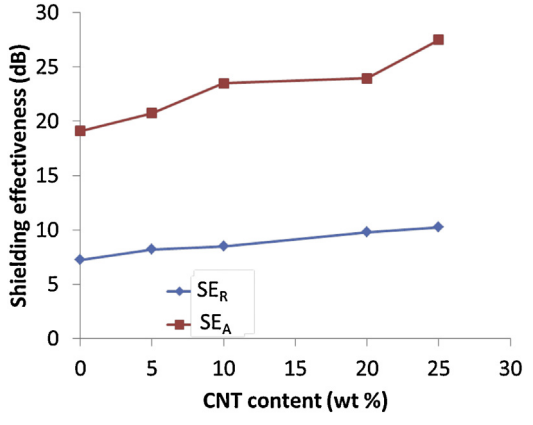

Fig. 3.6. Contribution of absorption (SE_A) and reflection (SE_R) to the SE of PANI/MWNTs nanocomposites prepared by in situ polymerization (thichness = 2 mm) [48].

However, these two techniques suffer from a highly expensive process step involving solvent drying and precipitation in a large quantity of non-solvent, that prevents industrial upscaling. Therefore, Thomassin et al. developed a new technique, called polymerization-precipitation, that consists in the polymerization of a monomer in the presence of CNTs in a poor solvent of the polymer [151]. During its formation, the polymer precipitates and entraps all the CNTs similar to a coagulation process but using a much lower amount of solvent. The PMMA/MWNTs nanocomposites prepared using this method were compared to materials obtained by melt-mixing and coagulation. The composites obtained by the polymerization-precipitation technique develop by far the highest electrical conductivity thanks to a better dispersion compared to coagulation and to a better preservation of the CNTs aspect ratio compared to the melt-mixing method (Fig. 3.8). Very high SE (>40 dB) was then achieved at only 2 wt% of CNTs (18–28 GHz, t = 7 mm).

Polymer emulsions have also been used to prepare CNTs nanocomposites for EMI shielding [152–156]. Li et al. have dispersed CNTs within a solution of styrene acrylic [152] and acrylic [153] emulsion particles to generate the nanocomposite film after evaporation of the solvent. Very low percolation thresholds (0.58 wt% in acrylic emulsion and 0.24 wt% in styrene acrylic emulsion) and very good shielding properties were obtained (20 dB at 8 wt% of CNTs, 8–12 GHz, ASTM D4935-99 for acrylic emulsion and 25 dB at 15 wt% of CNTs, 8–12 GHz, t = 2 mm for styrene acrylic emulsion). CNTs were also added during the emulsion polymerization of acrylic acid in presence of polyvinyl alcohol [154]. The composite microcapsules were not properly formed with pristine MWNTs. In contrast, after the introduction of polar groups to MWNTs with an oxyfluorination treatment, well-defined microcapsules were recovered with MWNTs preferentially localized within the shell of the particles. Consequently, the SE was significantly improved compared to the composite obtained with the pristine MWNTs (50 dB vs. 30 dB at 2.4 wt%, 0.8–4 GHz, ASTM D4935-99).

Similarly, CNTs were added during the polymerization dispersion of MMA [157]. MWNTs were first modified by partially

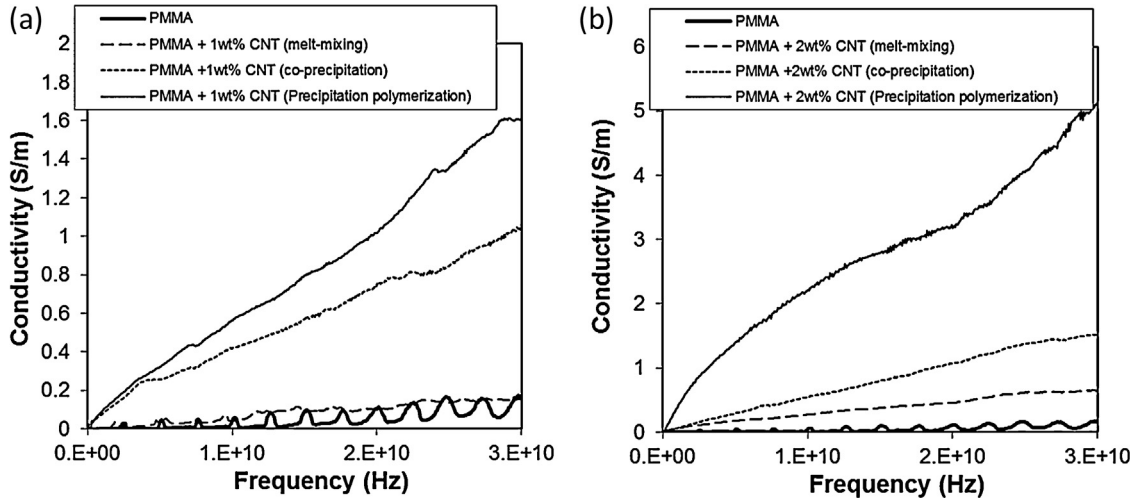

Fig. 3.8. Variation of the electrical conductivity σ' as a function of frequency for PMMA/CNTs nanocomposites prepared by melt-mixing, co-precipitation and precipitation polymerization techniques. (a) 1 wt% CNT and (b) 2 wt% CNT [151]. Reprinted from [151]. Copyright (2012), with permission from Elsevier.

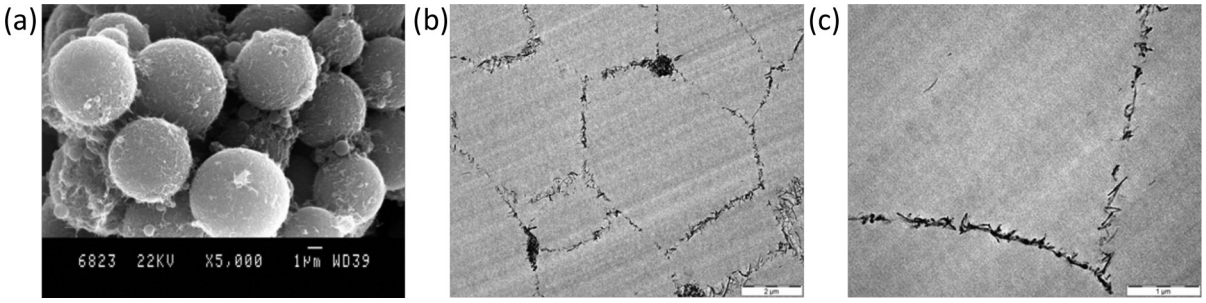

Fig. 3.9. (a) SEM micrographs, (b) and (c) TEM micrographs after compression molding of PMMA microspheres prepared by dispersion polymerization in presence of 1.66% of P(VAc-co-VA) (68% hydrolysis) and 1 wt% of CNTs-g-P(VAc-co-VA) [157]. Reprinted from [157]. Copyright (2010), with permission from The Royal Society of Chemistry.

hydrolyzed poly(vinyl acetate) via a radical process in order to impart surfactant properties to the carbon nanotubes. Only the modified CNTs (*CNTs-g-P(VAc-co-VA)* were able to stabilize the formation of the PMMA microspheres and were accordingly localized on their surface (Fig. 3.9a). Melt-compression of these microspheres led to the formation of a 3D network of connected CNTs (Fig. 3.9b and c) that presents a higher electrical conductivity compared to the nanocomposite prepared by dispersion of MWNTs within PMMA by melt-blending.

More specific dispersion methods, i.e. ball-milling (polyurethane) [158], paper making process (cellulose) [159], dispersion spraying (polystyrene) [160], and electrospinning (polyacrylonitrile) [161] have also been used for the preparation of EMI shielding materials with fairly good performances (Table 1). The ball-milling consists in inserting the different materials to mix in a cylindric container filled with ceramic or metallic balls that grind the samples into a very fine powder. A compression molding operation is then performed to obtain the EMI shielding material. In the paper making process, the carbon nanotubes are added in the aqueous solution of cellulose fiber in the presence of a cationic fixer. The water is then removed by pressing and drying to form the paper materials. The dispersion spraying technique consists in spraying a polymer/CNTs solution to quickly evaporate the solvent and to form the composite film. Finally, the electrospinning technique is based on electrostatic forces that draws out a jet of polymeric solution from a syringe under high voltage onto a conducting surface, resulting in thin nanofibers [162]. In the case of PAN composites prepared by electrospinning, the polymer is carbonized and is then electrically conductive. The addition of CNTs allows to reduce the electrical resistivity of the carbonized film and to achieve a 20 dB SE at 2 wt%.

3.4. Graphene sheets as conductive fillers

Graphene sheet (GS), a monolayer graphite, has attracted the attention of the scientific community in recent years thanks to excellent mechanical, thermal and electrical properties [163,164]. Moreover, due to its particular form, an atomically thick two-dimensional structure, the percolation threshold can be achieved at

Table 1
EMI SE of different polymer/MWNTs nanocomposites.

Dispersion method	Polymer matrix	CNT content (wt%)	Shielding effectiveness (dB)	Frequency (GHz)	Thickness (mm)	Reference
Ball-milling	PUR	22	20	8–12	0.1	[158]
Paper making process	cellulose	9.1	20	15–40	0.195	[159]
Dispersion spraying	PS	5	25	8–12	1	[160]
Electrospinning	PAN	2	20	0.3–3	0.150	[161]

Please cite this article in press as: J.-M. Thomassin, et al., Mater. Sci. Eng. R (2013), http://dx.doi.org/10.1016/j.mser.2013.06.001

very low content that makes graphene a suitable carbon filler for EMI shielding materials.

The first reported system [165] consisted in the dispersion of partially reduced graphene sheets into epoxy resin precursor followed by annealing of the film obtained by solvent casting at 250 °C to completely reduce the graphene sheets and to enhance the electrical conductivity. Very low percolation threshold was obtained (0.52 vol%), however a fairly large filler content was necessary to achieve a SE of 20 dB (15 wt%, 8–12 GHz). Bhattacharya et al. have demonstrated the higher efficiency of graphene sheets compared to carbon nanotubes when dispersed in polyurethane (8 dB vs. 5 dB at 10 wt% carbon filler loading, 8–12 GHz, $t = 2$ mm) [166]. However, a direct comparison of the effect of these two types of fillers on the SE performances of the corresponding materials would require additional experiments.

Graphene sheets were also dispersed within electrically conductive polymers (Poly(3-hexylthiophene) (P3HT) [167] and polyaniline [168–171]) in order to improve the shielding properties. Superhydrophobic P3HT/GS films were prepared by a solution deposition technique where drops of methanol were added to a chloroform solution of GS/P3HT which triggered P3HT aggregation and the rapid deposition onto the GS surface to form a surface with a high roughness [167]. While the presence of P3HT increases the hydrophobicity of the film, a decrease of the SE is observed when the P3HT content is increased due to a reduced contact between the GS. At equal concentration of P3HT and GS, the SE is superior to 20 dB (8–12 GHz, $t = 2$ mm). Graphene sheets were also demonstrated to further improve the shielding properties of polyaniline film compared to SWNTs (24.3 vs. 19.4 at 1 wt%, 0.45–1.5 GHz) [169]. A synergetic effect was observed when GS and SWNTs were combined thanks to the formation of a hybrid conductive network with SWNTs acting as conductive wires between the graphene sheets.

3.5. Summary

As explained in the introduction, a direct comparison between the performances of the nanocomposites based on the different carbon fillers is difficult to make because the measurements were performed at different frequencies and, more importantly, on samples involving different thicknesses. However, a general trend can be established by plotting the different SE reported in the literature as a function of the filler content and the kind of filler. Fig. 3.10 clearly shows that the highest SE are observed for carbon fillers with the highest aspect ratio (SWNTs > MWNTs > CNFs > CB). This observation is related to the ability of the fillers to impart electrical conductivities to the polymer matrix. In order to confirm this statement, the variations of the SE as a function of the DC conductivity has been compared for samples with the same

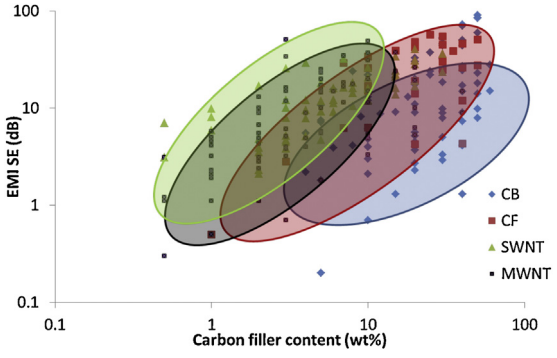

Fig. 3.10. reported SE as a function of the carbon filler content and of the kind of carbon filler.

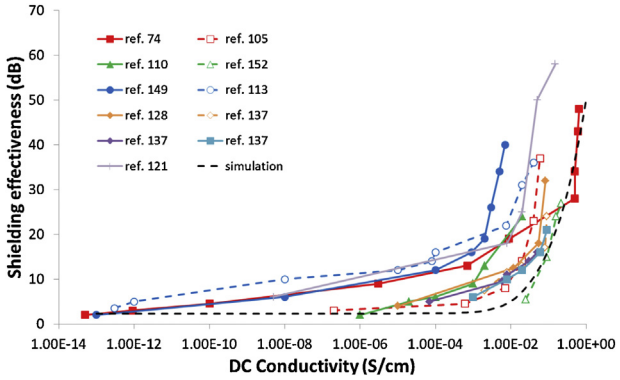

Fig. 3.11. SE (at 10 GHz) as a function of the DC conductivity for carbon particles based nanocomposites reported in references [74,105,110,113,121,128,137,149,152] (sample thickness around 2 mm).

thickness (about 2 mm). Although the absolute values cannot be directly compared, the general trends can be discussed. As shown in Fig. 3.11, the shielding effectiveness continuously increases with the DC conductivity. Two regimes can be distinguished. Firstly, just below the percolation threshold, the SE slightly increases with the conductive properties since in this regime a small change in carbon filler content dramatically increases the conductivity while the effect on the SE remains marginal. Secondly, after the percolation threshold, a small change in DC conductivity induces a large increase in shielding effectiveness because, at this stage, even if the conductivity does not significantly increase with the addition of carbon particles, the shielding properties become significantly sensitive to a small change in conductivity. The general tendency observed with the experimental data curves from literature corresponds quite well with the prediction (dashed curve) in the same frequency and thickness range, obtained using expression (2.17) from Section 2.2. Since the electrical conductivity and the percolation threshold are the key parameters for the achievement of high shielding effectiveness, the dispersion method should be chosen appropriately. During the dispersion, the carbon fillers should be disaggregated but not completely isolated. Contacts between carbon particles should indeed be preserved to ensure electrical conduction. For instance, the degree of agglomeration is a key parameter in carbon black composites to achieve percolation threshold at low filler content [172,173]. Appropriate mixing and annealing conditions should be accordingly used. Addition of salts in the nanocomposites favors also the agglomeration of carbon black particles and, consequently, decreases the percolation threshold [172,173]. For the other types of fillers, the preservation of large aspect ratio during the dispersion method is also required to achieve a low percolation threshold and, as a result, a high shielding effectiveness. Solution based dispersion methods are then preferable although they are more expensive compared to melt-processing. A ratio performance/cost should be taken into account for industrial applications. Other clues for the achievement of appropriate dispersion of these carbon fillers can be found in the different reviews dedicated on that subject (carbon black [174], carbon nanotube [175–178] and graphene [179–181]).

Some applications require that the materials should not only shield the electromagnetic radiation but should also limit the reflection at their surface. It is therefore important to determine which mechanisms, absorption (SE_A) or reflection (SE_R), have the dominant contribution to the total shielding effectiveness (equation 19). Several studies have shown that both contributions increase with the electrical conductivity, as expected (Fig. 3.12a). The increase in SE_A is more important than SE_R, which might suggest that the contribution of absorption to the SE increases with

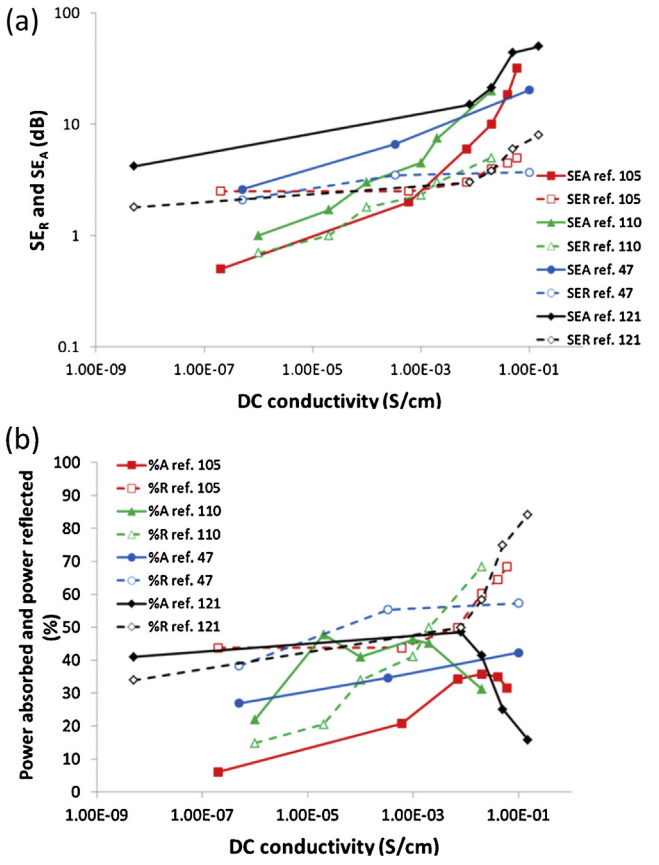

Fig. 3.12. (a) contribution of absorption (SE_A) and reflection (SE_R) to the total shielding effectiveness as a function of the DC conductivity and (b) percentage of power absorbed and power reflected as a function of the DC conductivity. All measurements were performed at 10 GHz with a sample thickness around 2 mm for references [47,105,110,121].

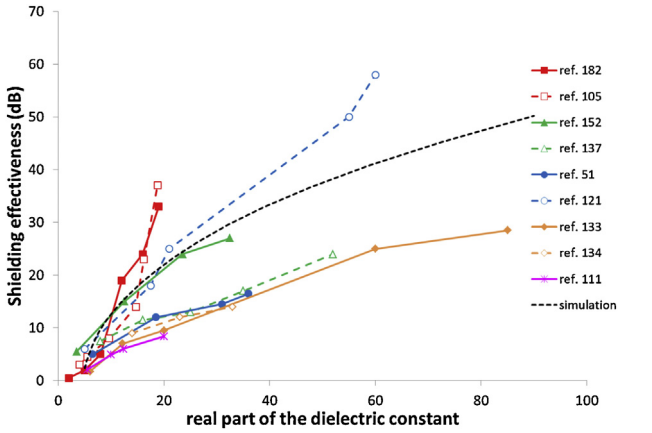

Fig. 3.13. SE (at 10 GHz) as a function of the dielectric constant for carbon particles based nanocomposites reported in references [51,105,111,121,133,134,137,152,182] (sample thickness around 2 mm).

the conductivity. However, since the reflection also increases with the filler content (due to the increase in dielectric constant as explained in Section 2.2) and occurs before the absorption, there is a lower proportion of the radiation left for absorption. This statement is demonstrated by plotting the level of power absorbed and reflected as a function of the conductivity (Fig. 3.12b). The proportion of the power truly absorbed by the materials reaches a maximum before decreasing at high electrical conductivity. It actually never surpasses 50% for these samples with a thickness of 2 mm. Indeed, although the absorption capacity is improved, there is a lower proportion of the radiation left for absorption after the intensive reflection associated to the high conductivity. A strategy based on increasing the conductivity (and therefore carbon filler loading) is then not an efficient way to prepare electromagnetic absorbers. Designing efficient EMI absorbers would require (1) maintaining a relatively low carbon fillers content (around the percolation threshold) in order to limit the reflection at the surface and (2) increasing the thickness of the samples. However this strategy is not appropriate for most applications due to the cost and geometric (or weight) constraints. Most of the strategies developed in Sections 4 and 5 are actually designed to overcome this issue.

Fig. 3.13 illustrates the dependence of SE on the value of the dielectric constant ε_r. Although, the values are different depending on the literature source, a global increase of the shielding performance with the dielectric constant is observed in each case as expected from the discussion in Section 2.2. Indeed, the proportion of the power reflected at input of the composite increases with this parameter. It is the result of the interfacial reflection coefficient Γ given by (2.14) that tends to unity with increasing dielectric constant, reducing accordingly the amount of power transmitted at output of the composite, thus inducing an increase of SE by virtue of (2.17). As for Fig. 3.11, the dashed line represents the prediction using (2.17) together with (2.14) for the involved interfacial reflection coefficient.

4. Combination with other kinds of fillers

This section presents EMI shielding materials based on polymer composites in which the carbon particles are modified and/or combined with another filler that also contributes to the shielding mechanism. It includes the coating of the carbon particles with a metallic layer, mainly to improve the electrical conductivity, the co-addition of metallic or metal oxide nanoparticles and the modification or co-addition of intrinsic conductive polymers.

4.1. Coating the carbon filler with metallic layers

In order to improve the electrical conductivity of carbon fillers and, consequently, their shielding performances, several authors have considered to coat the filler with a metallic layer. A large amount of papers have been dealing with the dispersion of metal-coated carbon fibers within acrylonitrile-butadiene-styrene co-polymer (ABS) [14,183–192]. Coating with nickel was the first studied system leading to improved EMI SE performances when compared to unmodified carbon fibers (45 dB vs. 30 dB at 23 wt%, 1 GHz, ASTM ES-7-83) thanks to a higher electrical conductivity [189]. Similarly to unmodified carbon particles, the preservation of the high aspect ratio of the coated fiber during the processing is a key parameter to achieve high SE and was highlighted by comparison of two kinds of melt-mixing procedures (internal mixer vs. extruder) [189], melt-mixing with solvent casting [191], by studying the effect of the screw speed [190] and by determining the influence of side-feeding the CNF during the melt-mixing process [190]. Tseng et al. have compared the coating of CNFs with copper and nickel on the shielding effectiveness of ABS composites [185]. Despite the fact that the resistivity of copper (0.017 μΩm) is much lower than nickel (0.073 μΩm), a better EMI SE was observed for the nickel coated fibers (30 dB vs. 15 dB, at 23 wt%, 0.03–1 GHz, ASTM ES-7-83). The main reason for this observation is attributed to the different fiber length distribution after processing which is in disfavor of the copper modified CNFs. Similar results were obtained by Huang et al. but they attributed

the lower performance of copper modified fillers to the higher sensitivity of copper to oxidation which alters its electrical conductivity [183]. In order to limit this drawback, they coated a second layer based on nickel-phosphorous more resistant to oxidation, leading to improved SE of the composites.

Nickel coated fibers were also dispersed within high impact polystyrene (HIPS), and their effect on the SE were compared to unmodified CNFs and polyurethane coated CNFs [193]. While the metallic coating induces a significant improvement (28 dB vs. 23 dB at 23 wt%, 1 GHz, ASTM ES7-83), the SE is reduced upon modification by polyurethane as a consequence of creating an insulating PU layer around CNFs that reduces the direct contact between carbon fibers (19 dB at 23 wt%, 1 GHz, ASTM ES7-83).

Carbon black was also modified with a nickel coating and dispersed within phenolic resin to achieve 50 dB SE at 23 wt% (1–15 GHz, $t = 1$ mm) [194]. Unfortunately, a comparison with unmodified carbon black is missing. The deposition of a metal coating (Ag and Ni) on carbon nanotubes was found to reduce the SE because the modification induces an aggregation of the CNTs and is therefore detrimental to the establishment of a conductive network [195].

Since this strategy mainly relies on the enhancement of the electrical conductivity of the filler, the nature of the coating must be selected in such a way that it improves this property while considering that the coating should not be detrimental to the quality of the carbon particles dispersion neither to their final aspect ratio.

4.2. Co-addition of metallic or metal oxide nanoparticles

In order to improve the shielding efficiencies of polymer/carbon particle nanocomposites, the parallel addition of metal or metal oxide particles has been largely envisioned. An improvement of the dielectric loss can be achieved but the main purpose lies in the enhancement of the magnetic permeability which increases the total energy of the radiation that can be truly absorbed by the materials. Moreover, by an appropriate combination of these two kinds of nanofillers, a better impedance match at the materials surface could be achieved which will reduce the overall EMI reflection. This strategy is popular in the design of microwave absorber and was widely described in a recent review [28]. The detailed results of the different approaches will thus not be described here and the reader is invited to read this excellent review by Qin et al. The main metallic or metal oxide particles envisioned are ferromagnetic (iron particle [196–205], iron nanorods [206], iron oxide [207–214], nickel nanoparticle [215–220], nickel nanowire [221], cobalt nanoparticle [222–224], their alloys [225–229], $La_{0.7}Sr_{0.3}MnO_{3-\delta}$ particle [230], carbonyl iron particle [231–233], NiZn ferrite particle [234], and hexaferrite [235–238]). Nonmagnetic particles (Ag [218,239], Sn [240], Er_2O_3 [241]) have been combined with carbon fillers as well with, however, a much lower improvement of the magnetic permeability. These latter particles are nevertheless efficient thanks to their ability to improve the dielectrical properties of the materials.

Carbon nanotubes have also been combined with MnO_2 nanotubes (MNT) in PVDF composites [242]. Since the conductivity of these nanofillers is two orders of magnitude lower than for MWNTs, they are not able to impart adequate shielding properties. However, by combining 5 wt% of MNTs with 1 wt% of MWNTs, similar SE to 7 wt% MWNTs can be achieved (20 dB, 8–12 GHz, $t = 10$ mm) but at a much lower cost. Moreover, the main mechanism associated to the presence of MNTs is by radiation absorption while reflection dominates for MWNTs. The absorption/reflection ratio can then be modulated by changing the relative amount of the two types of nanotubes.

4.3. Modification with intrinsic conductive polymer

As explained in the introduction, intrinsic conductive polymers can also be used as fillers for imparting electromagnetic shielding properties to conventional polymers. The combination of these fillers (polyaniline [243–246] and polypyrrole [247]) with carbon particles has also been envisioned by several research groups. The purpose of this strategy is to achieve enhanced electrical conductivity and shielding performances compared to the same material containing the separate fillers. In situ polymerization of the conducting polymer around the carbon particle is generally used prior to the dispersion of the combined fillers within the polymer matrix [243,245–247]. Separate dispersion of the two fillers is another possibility [244]. It has to be noted that synergetic effect of the two fillers is only observed when the conducting polymer does not negatively alter the dispersion of the carbon particles within the matrix.

As examples, MWNTs were modified by polypyrrole by in situ polymerization and added to an EVA polymer matrix [247]. A 35 dB SE was obtained when the content was 12.5 wt% in MWNTs and 17.4 wt% in PPY (1 GHz, ASTM D4935-99) while it was only 8 dB when the two fillers where added separately. The effective coating of MWNTs by PPY obtained during the in situ polymerization favors the creation of a conductive network. MWNTs were also combined with polyaniline and added to PEO based electrospun fibers [244]. The dispersion and adhesion of the MWNTs to PANI were improved using a fluorination treatment of MWNTs. A SE of 42 dB (0.8–8.5 GHz, ASTM 4935-99) was reached with absorption as the main shielding mechanism. Schettini et al. have recently mixed PANI and carbon black within styrene-b-(styrene-co-butadiene)-b-styrene) copolymer [246]. However, the presence of the intrinsic conducting polymer reduces the effectiveness of the carbon filler. They attribute this observation to the local de-doping of PANI due the basic nature of the carbon black particle.

5. Complex architectures of polymer/carbon based composites for EMI shielding

Starting from the polymer/carbon filler solid samples, more complex structures have been designed in order to improve the shielding performances. The main purpose is to reduce the reflectivity of the materials while keeping acceptable shielding properties. Indeed, the addition of carbon particles into a polymer matrix improves the electrical conductivity and the imaginary part of the permittivity which is beneficial for the absorption of the microwave radiation but the real part of the permittivity is also significantly increased which induces important reflection at the material surface.

5.1. Nanocomposite foams

Foaming the polymer composites can offer substantial advantages in shielding applications. First, the weight of the materials can be considerably decreased which is essential in some applications such as aircraft and telecommunication technologies. Secondly, even if the carbon fillers is diluted in volume, the concentration of particles within the cell walls of the foams keeps the average distance between them almost the same which is highly desirable when high electrical conductivity is searched for at low carbon filler loading. Finally, the presence of air inside the materials decreases the real part of the permittivity, consequently reducing the reflectivity at the material surface.

Yang et al. were the first to report on such systems based on polystyrene foams filled with carbon nanofibers [248] and carbon nanotubes [249]. The expansion of the materials was performed by mixing the polymer with a chemical foaming agent, i.e.

azoisobutyronitrile in solution. After spraying the solution on a flat plate, the film is thermally treated to induce the decomposition of the foaming agent. With this approach, a much higher EMI shielding can be achieved compared to copper metal sheets (33 vs. 10 dBcm^3/g, 8–12 GHz). The 20 dB shielding effectiveness is achieved at much lower filler content with carbon nanotubes compared to carbon fibers thanks to their higher aspect ratio (7 wt% vs. 20 wt%, 8–12 GHz). However, the reflectivity of the CNTs foams (T + A + R = 1 + 18 + 81%) is only slightly reduced compared to solid samples (T + A + R = 0.25 + 10.21 + 89.54%) and remains the main shielding mechanism probably due to a too high CNT content (7 wt%).

For polycaprolactone/CNTs nanocomposites [250] foamed by the supercritical CO_2 technology, a very high shielding effectiveness was obtained at very low CNT content (60 dB at 0.249 vol% and 20 dB at 0.107 vol%, t = 2 cm). This superior SE performance is the result of the excellent CNTs dispersion and of the improvement of the electrical conductivity upon foaming as exemplified by a foam containing 0.107 vol% MWNTs that presents the same conductivity as an unfoamed sample with 0.16 vol% MWNTs (Fig. 5.1a). Similarly, a foam with 0.249 vol% of MWNTs exhibits a conductivity twice that of an unfoamed sample filled with 0.48 vol% of MWNTs. Moreover, the introduction of air upon foaming leads to a lower dielectric constant for a given electrical conductivity. Indeed, the dielectric constant of foamed PCL filled with 0.24 vol% MWNT (ε_r = 3.5 at 30 GHz; Fig. 5.1c) is similar to those of unfoamed PCL containing 0.16 and 0.48 vol% MWNTs ($3 < \varepsilon_r < 4$; Fig. 5.1c), although the conductivity is roughly 3 to 4 times higher (Fig. 5.1b). Consequently, the foamed samples exhibit a better shielding effectiveness/reflectivity ratio (Fig. 5.1b and d).

Fletcher et al. have observed that the foaming of fluorocarbon elastomer/CNTs nanocomposites did not significantly decrease the SE while allowing a decrease of the density with potential weight savings of 23 to 30 wt% [251].

Other carbon fillers, such as carbon black within EPDM [252] and graphene sheets within PVDF [253] PUR [254], PS [255], PDMS [256] and PMMA [257] were used to prepare composite foams for EMI shielding application. Thanks to its high aspect ratio, incorporation of graphene sheets provide a 15 dB SE to PMMA foams at very low content (1.8 vol%, 8–12 GHz, t = 2.4 mm) with absorption as the main mechanism [257]. A lower percolation (in vol%) was achieved with the foamed samples compared to the solid ones, confirming the advantage of foaming. Yan et al. used the salt-leaching process to prepare PS foams with high content of graphene (30 wt%) to achieve a SE of 29 dB (8–12 GHz, t = 2.5 mm) [255] which corresponds to a specific shielding effectiveness of 64.4 dB/cm^3. Recently, Chen et al. used a nickel template to deposit graphene sheets by chemical vapor deposition. After coating the graphene layer with PDMS and etching away the template, highly flexible foams of low density (0.06 g/cm^3) were obtained and presented high specific EMI shielding effectiveness performances (500 dB/cm^3, 8–12 GHz, t = 1 mm) [256].

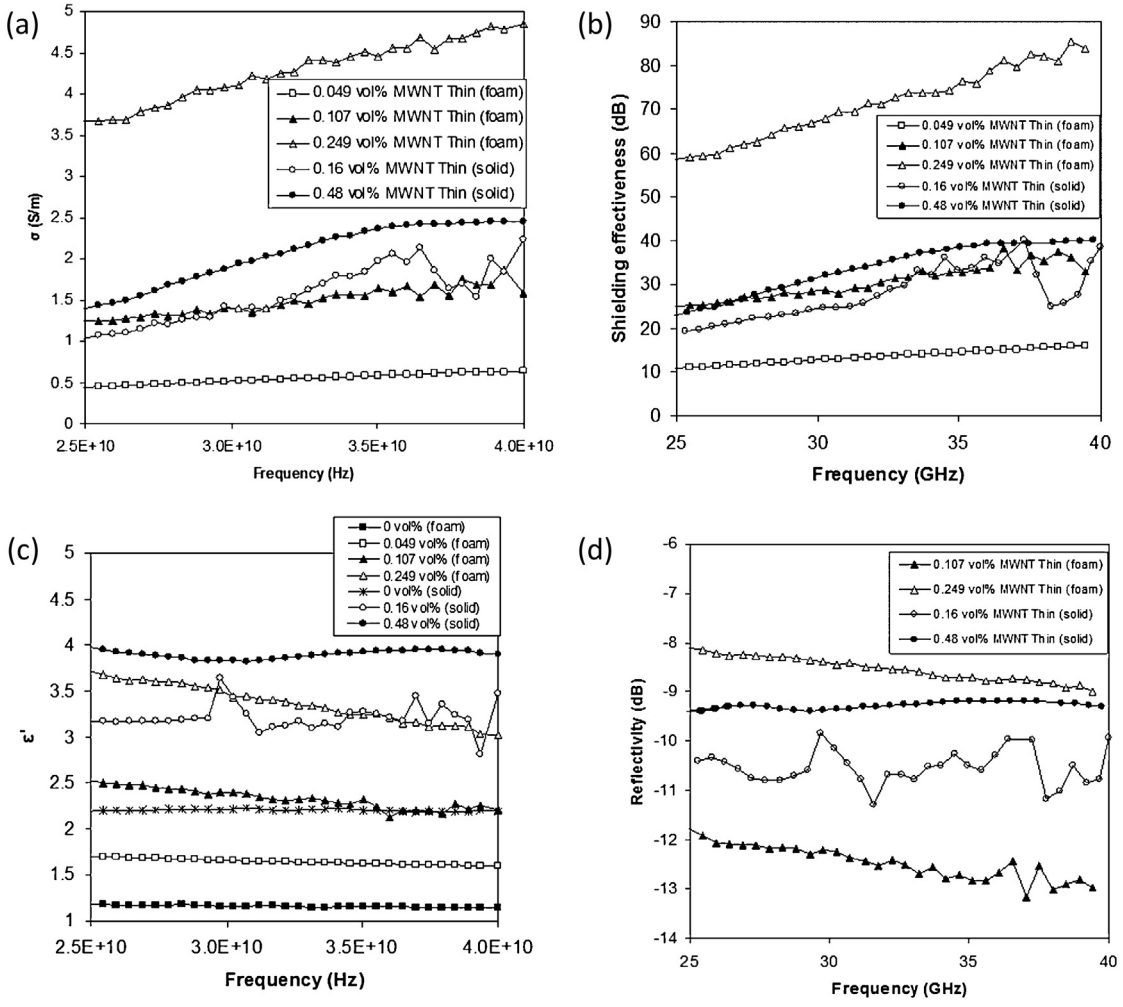

Fig. 5.1. Electromagnetic properties of foamed and unfoamed MWNT/PCL nanocomposites (a) conductivity σ' (b) shielding efficiency SE, (c) dielectric constant ε_r, (d) Reflectivity R [250]. Reprinted from [250]. Copyright (2008), with permission from The Royal Society of Chemistry.

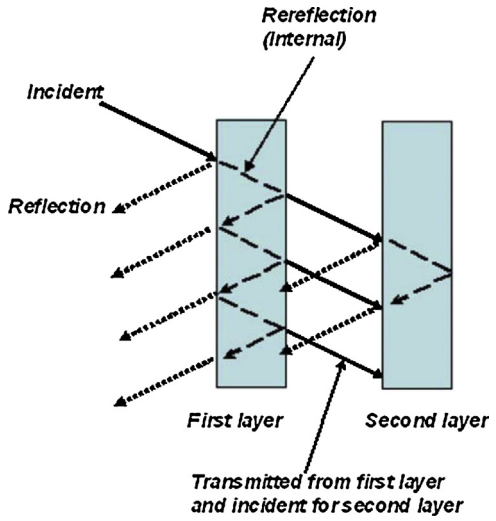

Fig. 5.2. Principle of multi-reflection in a multilayered structure.

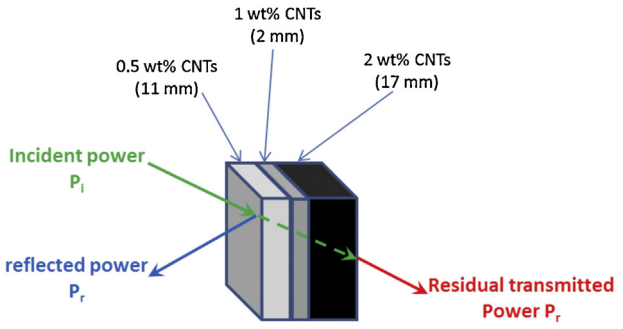

Fig. 5.3. Principle of multi-layered PCL/CNTs foams with a gradient in CNTs content.

5.2. Multilayers

Another way to further improve the shielding effectiveness/reflectivity ratio is to prepare multilayered structures. Two different cases must be distinguished. The first one simply consists to stack different layers of polymer composites with the same concentration of carbon particles. The improvement results here from an increase of the multi-reflection mechanism as depicted in Fig. 5.2. While the presence of multi-reflection increases the total reflection, the impact on the apparent absorption is dominant which results in higher SE/reflectivity ratio. This strategy has been proved efficient for PMMA [258,259] and epoxy [136] nanocomposites.

The second method relies on the use of a multi-layered structure in which the carbon filler content is gradually increased from one layer to the next one. The main objective is to avoid the presence of an interface between two media with large difference in dielectric constant ε_r and thus to limit the reflectivity at each interface [260,261]. This technique was combined with the foam strategy [261] (see Section 5.1) through face-to-face assembly of three slices of foams of increasing CNTs concentrations and different thicknesses: 0.5 wt% (11 mm)/1 wt%(2 mm)/2 wt%(17 mm) (see Fig. 5.3). The average CNTs concentration in this three-layered foam was 1.38 wt%. The thickness of the first layer (low CNT concentration and dielectric constant) is about one third of the total thickness t to ensure a smooth penetration of the signal into the composite, while the thin second layer of intermediate concentration aims to match the low dielectric constant of first layer to the higher dielectric constant of the third layer. The thickness of the latter is maximized (about 2/3 of total thickness) in order to optimize the power dissipation in its highly conductive structure.

The bold solid curve in Fig. 5.4a shows that the shielding effectiveness of the three-layered foam is comparable to that of a monolayer with the same thickness and a similar CNTs concentration (1 wt%, dashed curve). In contrast, the total reflection by the multilayer was decreased by at least 5 dB, thus by approximately 70%, compared to the same monolayer (1 wt%, dashed curve, Fig. 5.4b). Moreover, the graded concentration also ensures that the decrease of reflection is observed over a broad frequency range (restricted to 28 GHz in this study, due to measurement constraints), and not only at discrete frequencies as for Salisbury screens that present a reflection lower than −10 dB over less than 2 GHz bandwidth [262].

For the sake of completeness, another hybrid multi-layered structure, widely used as radar absorbing material (RAM) and popularized under the name "Salisbury screen", has to be briefly discussed. It consists in stacking a metallic backing plane, a dielectric insulating layer of thickness t (usually called "spacer"), and a thin covering conductive layer. Depending on the operating frequency, i.e. when the thickness t is an odd multiple of quarter wavelengths, signals respectively entering the structure and reflected back by the metal plane compensate themselves in such a manner that only the equivalent resistance of the conductive sheet is seen by the incoming wave. Adjusting this resistance to the

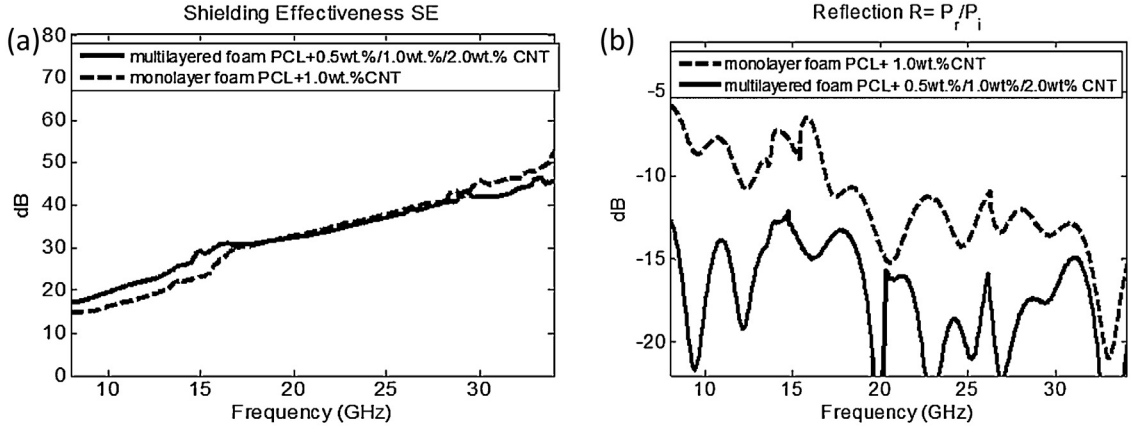

Fig. 5.4. (a) Shielding effectiveness and (b) reflection of CNTs/PCL foams (30 mm thick) of a single CNTs concentration: 1 wt% (dashed), compared to a three layered sample with a graded CNTs concentration (bold lines): 0.5 wt% (11 mm)/1 wt% (2 mm)/2 wt% (17 mm).

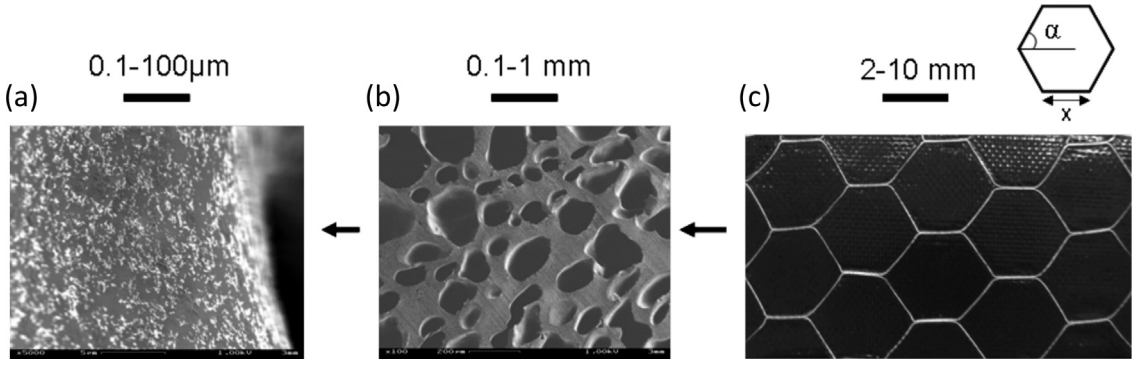

Fig. 5.5. Multimaterial and multiscale strategy developed to reach high EM absorption levels in the GHz range starting from (a) CNT dispersed in a polymer matrix which is (b) foamed and (c) inserted in a metallic honeycomb. Reprinted from [49]. Copyright (2012), with permission from IEEE.

377 Ohms impedance of air cancels any reflection from a target behind the metal plane. Two comments must be added. Firstly, this sandwich structure is only efficient at discrete frequencies corresponding to multiple quarter wavelengths, meaning that the choice of the dielectric constant of the spacer material will fix these frequencies. Variant of Salisbury screens, called Jaumann absorbers, use a stack of layers with varying permittivity enabling to enlarge somewhat the bandwidth, at the price of an increase of the total thickness. Secondly, any kind of conductive particle is admissible for the resistive/conductive cover sheet: carbon black, carbon fiber, or carbon nanotubes as recently tested [263].

5.3. Honeycombs

As explained in the previous sections, foamed conductive composites are good candidates for making microwave absorbers. Monolayer or multilayered foamed structures have been developed with various shapes as radar absorbing materials [264]. The most popular one is the pyramidal shape, widely used in anechoic chambers. This particular progressive profile minimizes reflection for any incoming angle of the wave over a large frequency range depending on the geometry of the pyramid. Another shape of interest for wide incidence angle is the hollow foamed honeycomb, i.e. a honeycomb lattice grid using a conductive dielectric as cell walls. But the honeycomb geometry is also known in EMI applications for two other properties: as mechanical stiffening constituents in sandwich or in multilayered absorbing panels, or as shields exploiting the waveguiding properties of metallic honeycomb cells below or above cut-off. The use of a foam filled honeycomb inside a sandwich configuration for enhanced mechanical performances has already been studied in the literature [265–267]. David et al., proposed Salisbury and Jauman absorbers with as dielectric slab a unfilled honeycomb reinforcing dielectric structure [268]. Fan et al. [269] considered a carbon black loaded foamed slab reinforced by a Glass Fiber Reinforced Concrete (GFRC) honeycomb-like lattice grid. Reflectivity measurements showed that the insertion of the lattice in the conductive foamed layer does not damage the absorbing performances of the resulting structure. On the other hand, the shielding operation of metallic air vents made of honeycomb arrays is well known: they are used as substitutes to fully reflective metal plates for blocking transmission of EM signals [270] while allowing air flow, heat convection/radiation, etc. Their particular operation is governed by the existence of a cut-off frequency which is a function of the aperture size of the honeycomb cell. The following expression has been derived [49] and validated by experiment for the equivalent dielectric constant and conductivity of a hybrid slab made of a foamed conductive slab inserted into a honeycomb with metallic surfaces, see Fig. 5.5:

$$\varepsilon_{\mathrm{effh}} = \varepsilon_{\mathrm{r,fill}} - \frac{5}{8}\left(\frac{\pi c_o}{X\omega}\right)^2 - \frac{j\sigma_{\mathrm{fill}}}{\omega\varepsilon_o} \tag{5.1}$$

where ω is the radiant pulsation $2\pi f$, c_o is the velocity of light in air, X is the honeycomb cell size, ε_0 is the permittivity of vacuum, $\varepsilon_{\mathrm{rfill}}$ is the relative permittivity, and σ_{fill} is the electrical conductivity (real part) of the material filling the honeycomb cells, respectively. As explained in details in [49,271], the presence of the honeycomb acts as a waveguide providing a synergy effect with the response of the interior material, that can be air (as in EMI shielding air vents) or any other material, absorbing or not. Expression (5.1) and Fig. 5.6a

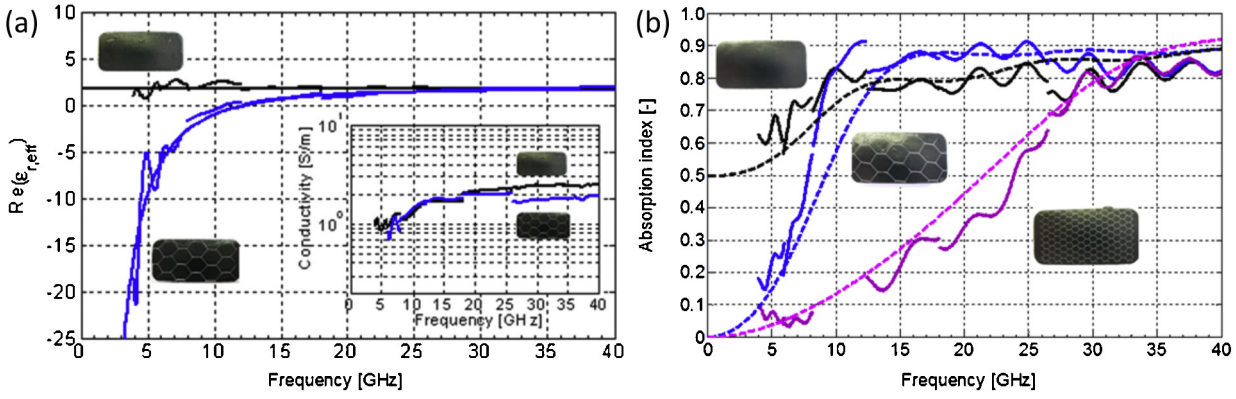

Fig. 5.6. Measured (solid lines) and predicted (dashed lines) (a) effective dielectric constant provided by expression (5.1) and (b) absorption provided by expression (2.11) versus frequency for 7 mm thick PC-CNT 1 wt% foam and the corresponding hybrids with X = 4.76 mm and 1.58 mm. Reprinted from [49]. Copyright (2012), with permission from IEEE.

show that effective permittivity values lower than zero can be attained for operating frequencies lower than a cut-off frequency equal to $f_c = (5/16)c_o/X/\sqrt{\varepsilon_{rfill}}$: the cut off frequency decreases proportional to the increase of cell size X. Negative values mean that the equivalent medium formed by the hybrid has a purely imaginary wave impedance $\sqrt{\mu/\varepsilon}$ and purely real complex propagation constant as defined in Section 2; the propagation is stopped and the honeycomb structure acts, below cut-off, as a fully reflective shield.

As explained in Sections 3 and 4, the different strategies of architecturing the composite by foaming and/or by producing a gradient of microstructure in multilayers is a first route toward lowering the permittivity. An optimum absorption performance should be attained when the dielectric constant of the medium is close to 1, since, in that case, the reflection and the reflectivity should be minimum. Fig. 5.6a and equation (5.1) further reveal that the equivalent dielectric constant seen by the wave passing through the waveguide structure $\left(\Re_{(\varepsilon_{effw})}\right)$, being negative below the cut-off frequency, recovers to positive values above it, but remains always lower than the dielectric constant ε_{rfill} of the filling material. Considering that the hybrid structure (nanocomposite foam + honeycomb) is surrounded by air having permittivity equal to unity, it can be predicted that the power reflected by the hybrid structure should, above the cut-off, always be lower than the power reflected by the same composite without honeycomb, meaning that the absorption will be superior in the presence of a waveguide by virtue of the power balance (2.10–2.11). Fig. 5.6b gives an example of the variation of the absorbed power (2.11) as a function of the frequency for a polycarbonate foam with 1% CNT with or without a honeycomb structure. As expected, the presence of the honeycomb improves the absorption above the cut off frequency, here located at about 10 and 30 GHz for 4.76 and 1.58 mm cell sizes X, respectively. A variety of these hybrid materials have indeed been processed, made of CNT reinforced polymers foams in aluminum honeycomb, involving different matrices, amount of CNT and honeycomb cell and thickness dimensions, as well as different processing routes [49,271,272]. Foaming can be performed inside the honeycomb by using supercritical CO_2 as physical foaming agent or by chemical foaming. Another technique consists in inserting mechanically the foam inside the honeycomb with a press and by heating up the system for rheological reasons. Fig. 5.6 also shows that experimental results for the absorption A are in excellent agreement with the theoretical formalism detailed in Section 2, provided that expression (5.1) is used for the complex permittivity of the composite involved in the formulas. This analytical formalism provides the mathematical foundation for further optimizing the EM absorption of the hybrid using honeycomb with varying cell sizes for applications involving the protection to a wide range of frequencies, as further illustrated in [49,271].

The use of a honeycomb filled with a polymer foam has other advantages in addition to enhancing the EM absorbing performances. First, some applications, such as in power electronics shielding, require thermal management. The heat must be evacuated. A polymer foam is a good thermal insulator. A few % of CNT do not appreciably raise the thermal conductivity [273]. A metallic honeycomb, the most obvious being made of aluminum, can significantly increase the effective thermal conductivity and therefore the dissipation inside the material [271]. On the contrary, when high thermal insulation is targeted, a composite or polymer honeycomb (like Nomex) can be used with metallized surfaces. Secondly, the filled honeycomb hybrid material provides interesting stiffness characteristics that can be efficiently used only in the context of sandwich panels, as explained before and illustrated in [272] where structures similar to Fig. 5.5c are used as the core of a sandwich structure.

6. Conclusions

The different strategies developed to prepare EMI shielding materials based on polymer/carbon particles composites have been reviewed. In order to make an efficient screen, the materials must exhibit moderately high electrical conductivity (typically σ' near 1 S/m) and/or high dielectric constant. These requirements are reached when the carbon particles are appropriately dispersed inside the polymer with the establishment of a 3D network and a close contact between the particles. Consequently, the aspect ratio of the fillers is a key parameter and is determinant for the relative efficiency of the different fillers that can be ranked as: carbon black < carbon fiber < carbon nanotube < graphene sheet. The dispersion method is another important factor and must preserve the high aspect ratio of the fillers as much as possible while ensuring an adequate distribution of the carbon particles within the polymer matrix. A solution processing is then generally more efficient compared to melt-mixing characterized by high shears that are damageable for the fillers length. When melt-mixing is concerned, the process parameters like temperature, mixing time and screw speed have to be optimized to provide a good compromise between an ideal dispersion and the preservation of the aspect ratio of the carbon particles. Since the most efficient filler and the best dispersion method are also the most expensive, a compromise between shielding effectiveness and cost should also be taken into account for designing useful applications. The most appropriate candidates will depend on the requirement of each specific application. However, it must be pointed out that choosing cheap carbon particles will most often result in the need of very high filler contents that may damage other materials properties.

Different strategies have been envisioned in order to improve the performances of carbon particles/polymer composites. They include the metallic coating of the carbon particles, the co-addition of metallic nanoparticles or intrinsic conductive polymer and the development of complex structures. The most advanced material architectures for EM absorption comprise foams, multilayered, woven structures and incorporation of the polymer composite within a metallic honeycomb.

Acknowledgements

The authors thank the EU in the frame of the 7th Framework Program research project "HARCANA" (Grant Agreement No: NMP3-LA-2008-213277), the Fonds National de la Recherche Scientifique (F.R.S.-F.N.R.S., Belgium) for financial supports, the "Belgian Science Policy" in the frame of the "Interuniversity Attraction Poles Program (PAI VI/27)-Functional Supramolecular Systems" for financial support, the Region Wallonne in the frame of the WINNOMAT II "MULTIMASEC" research program. The University of Liege and French Community is also acknowledged for financial support in the frame of the "Action de recherche concertée" (ARC) research program "Bridging".

References

[1] X. Colin Tong, Advanced Materials and Design for Electromagnetic Interference Shielding, Taylor & Francis Group, 2009.
[2] S. Geetha, K.K.S. Kumar, C.R.K. Rao, M. Vijayan, D.C. Trivedi, J. Appl. Polym. Sci. 112 (2009) 2073–2086.
[3] R.M. Bagwell, J.M. McManaman, R.C. Wetherhold, Compos. Sci. Technol. 66 (2006) 522–530.
[4] K.K. Biswas, S. Somiya, Mater. Sci. Res. Int. 7 (2001) 172–177.
[5] C.-S. Chen, W.-R. Chen, S.-C. Chen, R.-D. Chien, Int. Commun. Heat Mass Transfer 35 (2008) 744–749.
[6] S.-T. Tan, M.-Q. Zhang, M.-Z. Rong, H.-M. Zeng, Polym. Compos. 20 (1999) 406–412.
[7] R.C. Wetherhold, R.M. Bagwell, J.M. McManaman, MD (Am. Soc. Mech. Eng.) 99 (2004) 1–6.
[8] V.J. Babu, V.S.P. Kumar, B. Sundaray, V.R.K. Murthy, T.S. Natarjan, Mater. Sci. Eng., B 142 (2007) 46–50.

[9] K.-S. Chou, K.-C. Huang, Z.-H. Shih, J. Appl. Polym. Sci. 97 (2005) 128–135.
[10] C.-J. Huang, T.-C. Chang, J. Appl. Polym. Sci. 91 (2004) 270–273.
[11] C.-J. Huang, F.-S. Shieu, Jpn. J. Appl. Phys., Part 1 42 (2003) 5336–5341.
[12] B.-W. Li, Y. Shen, Z.-X. Yue, C.-W. Nan, Appl. Phys. Lett. 89 (2006) 132503, 132504/132501-132504/.
[13] Y. Yang, M.C. Gupta, K.L. Dudley, Micro Nano Lett. 2 (2007) 85–89.
[14] S.Y. Yang, C.Y. Chen, S.H. Parng, Polym. Compos. 23 (2002) 1003–1013.
[15] S.H. Jang, S.W. Byun, S.H. Kim, PMSE Prepr. 86 (2002) 173–174.
[16] H.K. Kim, S.W. Byun, S.H. Jeong, Y.K. Hong, J.S. Joo, K. Song, Y.H. Park, J.Y. Lee, Mol. Cryst. Liq. Cryst. Sci. Technol., Sect. A 377 (2002) 369–372.
[17] H.K. Kim, M.S. Kim, S.Y. Chun, Y.H. Park, B.S. Jeon, J.Y. Lee, Y.K. Hong, J. Joo, S.H. Kim, Mol. Cryst. Liq. Cryst. 405 (2003) 161–169.
[18] M.S. Kim, H.K. Kim, S.W. Byun, S.H. Jeong, Y.K. Hong, J.S. Joo, K.T. Song, J.K. Kim, C.J. Lee, J.Y. Lee, Synth. Met. 126 (2002) 233–239.
[19] S. Bhadra, N.K. Singha, D. Khastgir, Polym. Eng. Sci. 48 (2008) 995–1006.
[20] Y. Duan, S. Liu, H. Guan, Sci. Technol. Adv. Mater. 6 (2005) 513–518.
[21] Y. Duan, S. Liu, H.J. Guan, Compos. Mater. 40 (2006) 1093–1104.
[22] S. Geetha, K.K.S. Kumar, D.C. Trivedi, J. Compos. Mater. 39 (2005) 647–658.
[23] K. Lakshmi, H. John, K.T. Mathew, R. Joseph, K.E. George, Acta Mater. 57 (2009) 371–375.
[24] Y. Niu, Polym. Compos. 27 (2006) 627–632.
[25] S. Vulpe, F. Nastase, C. Nastase, I. Stamatin, Thin Solid Films 495 (2005) 113–117.
[26] S. Courric, V.H. Tran, Polym. Adv. Technol. 11 (2000) 273–279.
[27] T. Taka, Synth. Met. 41 (1991) 1177–1180.
[28] F. Qin, C.J. Brosseau, Appl. Phys. 111 (2012), 061301/061301-061301/061324.
[29] S. Barrau, P. Demont, A. Peigney, C. Laurent, C. Lacabanne, Macromolecules 36 (2003) 5187–5194.
[30] B.E. Kilbride, J.N. Coleman, J. Fraysse, P. Fournet, M. Cadek, A. Drury, S. Hutzler, S. Roth, W.J. Blau, J. Appl. Phys. 92 (2002) 4024–4030.
[31] J.K.W. Sandler, J.E. Kirk, I.A. Kinloch, M.S.P. Shaffer, A.H. Windle, Polymer 44 (2003) 5893–5899.
[32] S. Kirkpatrick, Rev. Mod. Phys. 45 (1973) 574–588.
[33] L. Flandin, M. Verdier, B. Boutherin, Y. Brechet, J.Y. Cavaille, J. Polym. Sci. Part B: Polym. Phys. 37 (1999) 805–814.
[34] D. Stauffer, Introduction to Percolation Theory, Taylor & Francis, London, 1985.
[35] P. Potschke, S.M. Dudkin, I. Alig, Polymer 44 (2003) 5023–5030.
[36] G. He, J. Zhou, K. Tan, H. Li, Compos. Sci. Technol. 71 (2011) 1914–1920.
[37] B.-K. Zhu, S.-H. Xie, Z.-K. Xu, Y.-Y. Xu, Compos. Sci. Technol. 66 (2006) 548–554.
[38] A.N. Lagarkov, A.K. Sarychev, Phys. Rev. B: Condens. Matter. 53 (1996) 6318–6336.
[39] C.A. Grimes, C. Mungle, D. Kouzoudis, S. Fang, P.C. Eklund, Chem. Phys. Lett. 319 (2000) 460–464.
[40] I. Balberg, C. Anderson, S. Alexander, N. Wagner, Phys. Rev. B 30 (1984) 3933–3943.
[41] J.-B. Kim, S.-K. Lee, C.-G. Kim, Compos. Sci. Technol. 68 (2008) 2909–2916.
[42] D. Rodney, M. Fivel, R. Dendievel, Phys. Rev. Lett. 95 (2005) 108004, 108004/108001-108004/.
[43] J.P. Clerc, G. Giraud, J.M. Laugier, J.M. Luck, Adv. Phys. 39 (1990) 191–309.
[44] A. Saib, L. Bednarz, R. Daussin, C. Bailly, X. Lou, J.-M. Thomassin, C. Pagnoulle, C. Detrembleur, R. Jerome, I. Huynen, IEEE Trans. Microwave Theory Tech. 54 (2006) 2745–2754.
[45] A. Sivhola, Electromagnetic Mixing Formula and Applications, IEE Press, 1999.
[46] J. Joo, C.Y. Lee, J. Appl. Phys. 88 (2000) 513–518.
[47] M.H. Al-Saleh, U. Sundararaj, Carbon 47 (2009) 1738–1746.
[48] P. Saini, V. Choudhary, B.P. Singh, R.B. Mathur, S.K. Dhawan, Mater. Chem. Phys. 113 (2009) 919–926.
[49] N. Quiévy, P. Bollen, J.M. Thomassin, C. Detrembleur, T. Pardoen, C. Bailly, I. Huynen, IEEE Transactions on Electromagnetic Compatibility 54 (Special Issue on Nanotechnology) (2012) 43–51.
[50] W.S. Jou, T.L. Wu, S.K. Chiu, W.H. Cheng, J. Electron. Mater. 30 (2001) 1287–1293.
[51] Z. Liu, G. Bai, Y. Huang, Y. Ma, F. Du, F. Li, T. Guo, Y. Chen, Carbon 45 (2007) 821–827.
[52] N.B. Janda, J.M. Keith, J.A. King, W.F. Perger, T.J. Oxby, J. Appl. Polym. Sci. 96 (2005) 62–69.
[53] I. Huynen, C. Steukers, F. Duhamel, IEEE Trans. Instrum. Meas. 50 (2001) 1343–1348.
[54] A.A. Barba, G. Lamberti, M. d'Amore, D. Acierno, Polym. Bull. (Heidelberg, Ger.) 57 (2006) 587–593.
[55] I. Huynen, L. Bednarz, J.M. Thomassin, C. Pagnoulle, R. Jerome, C. Detrembleur, in: Proceedings of the 38th European Microwave Conference, 2008.
[56] J. Sanchez-Gonzalez, A. Macias-Garcia, M.F. Alexandre-Franco, V. Gomez-Serrano, Carbon 43 (2005) 741–747.
[57] P. Ghosh, A. Chakrabarti, Eur. Polym. J. 36 (2000) 1043–1054.
[58] G.T. Mohanraj, T.K. Chaki, A. Chakraborty, D. Khastgir, Polym. Eng. Sci. 46 (2006) 1342–1349.
[59] B.P. Sahoo, K. Naskar, D.K. Tripathy, J. Mater. Sci. 47 (2012) 2421–2433.
[60] O.A. Al-Hartomy, F. Al-Solamy, A. Al-Ghamdi, N. Dishovsky, V. Iliev, F. El-Tantawy, Int. J. Polym. Sci. (2011), 837803, 837807 pp.
[61] M. Rahaman, T.K. Chaki, D.J. Khastgir, Mater. Sci. 46 (2011) 3989–3999.
[62] M. Madani, J. Polym. Res. 17 (2010) 53–62.
[63] F.J. El-Tantawy, Appl. Polym. Sci. 97 (2005) 1125–1138.
[64] Q. Ling, J. Sun, Q. Zhao, Q. Zhou, Polym. Plast. Technol. Eng. 50 (2011) 89–94.
[65] D.H. Kim, D.I. Kim, C.M. Choi, J. Korean Phys. Soc. 56 (2010) 1109–1113.
[66] M. Al-Saleh, U. Sundararaj, J. Phys. D: Appl. Phys. 46 (2013), 035304/035301-035304/035307.
[67] J.-H. Oh, K.-S. Oh, C.-G. Kim, C.-S. Hong, Compos. Part B: Eng. 35B (2004) 49–56.
[68] M.E. Achour, C. Brosseau, F.J. Carmona, Appl. Phys. 103 (2008), 094103/094101-094103/094110.
[69] M.H. Al-Saleh, U. Sundararaj, Macromol. Mater. Eng. 293 (2008) 621–630.
[70] M.H. Al-Saleh, U. Sundararaj, Carbon 47 (2009) 2–22.
[71] G.G. Tibbetts, M.L. Lake, K.L. Strong, B.P. Rice, Compos. Sci. Technol. 67 (2007) 1709–1718.
[72] N.C. Das, D. Khastgir, T.K. Chaki, A. Chakraborty, Composites, Part A 31A (2000) 1069–1081.
[73] N.C. Das, T.K. Chaki, D. Khastgir, A. Chakraborty, Adv. Polym. Technol. 20 (2001) 226–236.
[74] N.C. Das, T.K. Chaki, D. Khastgir, A.J. Chakraborty, Appl. Polym. Sci. 80 (2001) 1601–1608.
[75] N.C. Das, D. Khastgir, T.K. Chaki, A.J. Chakraborty, Elastomers Plast. 34 (2002) 199–223.
[76] P.B. Jana, A.K. Mallick, S.K. De, Composites 22 (1991) 451–455.
[77] P.B. Jana, A.K. Mallick, S.K. De, J. Mater. Sci. 28 (1993) 2097–2104.
[78] J.A. Heiser, J.A. King, J.P. Konell, L.L. Sutter, Polym. Compos. 25 (2004) 407–416.
[79] J.M. Keith, N.B. Janda, J.A. King, W.F. Perger, T.J. Oxby, Polym. Compos. 26 (2005) 671–678.
[80] Q.J. Krueger, J.A. King, Adv. Polym. Technol. 22 (2003) 96–111.
[81] V. Sridhar, D. Xu, D.K. Tripathy, J.K. Kim, e-Polym (2008), No pp given.
[82] L. Nayak, D. Khastgir, T.K. Chaki, J. Mater. Sci. 48 (2013) 1492–1502.
[83] M.H. Al-Saleh, U. Sundararaj, Polymer 51 (2010) 2740–2747.
[84] M.H. Al-Saleh, U. Sundararaj, Polym. Adv. Technol. 22 (2011) 246–253.
[85] M. Rahaman, T.K. Chaki, D. Khastgir, Polym. Compos. 32 (2011) 1790–1805.
[86] W.S. Jou, T.L. Wu, S.K. Chiu, W.H. Cheng, J. Electron. Mater. 31 (2002) 178–184.
[87] B.O. Lee, W.J. Woo, H.S. Park, H.S. Hahm, J.P. Wu, M.S. Kim, J. Mater. Sci. 37 (2002) 1839–1843.
[88] B.O. Lee, W.J. Woo, H.S. Song, H.-S. Park, H.-S. Hahm, J.-P. Wu, M.-S. Kim, J. Ind. Eng. Chem. (Seoul Republic of Korea) 7 (2001) 305–309.
[89] B.O. Lee, W.J. Woo, M.-S. Kim, Macromol. Mater. Eng. 286 (2001) 114–118.
[90] J. Wu, D.D.L. Chung, Carbon 40 (2002) 445–447.
[91] T. Zou, N. Zhao, C. Shi, J. Li, Bull. Mater. Sci. 34 (2011) 75–79.
[92] F. Nanni, P. Travaglia, M. Valentini, Compos. Sci. Technol. 69 (2009) 485–490.
[93] X. Lv, S. Yang, J. Jin, L. Zhang, G. Li, J. Jiang, J. Macromol. Sci. Part B: Phys. 49 (2010) 355–365.
[94] B.P. Singh, V. Choudhary, P. Saini, R.B. Mathur, AIP Adv. 2 (2012), 4730043, 4730047 pp.
[95] E.G. Gamaly, T.W. Ebbesen, Phys. Rev. B: Cond. Matter 52 (1995) 2083–2089.
[96] Z. Shi, Y. Lian, X. Zhou, Z. Gu, Y. Zhang, S. Iijima, L. Zhou, K.T. Yue, S. Zhang, Carbon 37 (1999) 1449–1453.
[97] S. Iijima, Nature (London, U.K.) 354 (1991) 56–58.
[98] S. Iijima, T. Ichihashi, Nature (London) 363 (1993) 603–605.
[99] W.K. Maser, E. Munoz, A.M. Benito, M.T. Martinez, G.F. de la Fuente, Y. Maniette, E. Anglaret, J.L. Sauvajol, Chem. Phys. Lett. 292 (1998) 587–593.
[100] C.D. Scott, S. Arepalli, P. Nikolaev, R.E. Smalley, Appl. Phys. A: Mater. Sci. Process. 72 (2001) 573–580.
[101] A. Thess, R. Lee, P. Nikolaev, H. Dai, P. Petit, J. Robert, C. Xu, Y.H. Lee, S.G. Kim, et al. Science (Washington, D. C.) 273 (1996) 483–487.
[102] J. Kong, A.M. Cassell, H. Dai, Chem. Phys. Lett. 292 (1998) 567–574.
[103] Z.F. Ren, Z.P. Huang, J.W. Xu, J.H. Wang, P. Bush, M.P. Siegel, P.N. Provencio, Science (Washington, D. C.) 282 (1998) 1105–1107.
[104] A. Gupta, V. Choudhary, PMSE Prepr. (2010), No pp given.
[105] A. Gupta, V. Choudhary, Compos. Sci. Technol. 71 (2011) 1563–1568.
[106] A. Gupta, V.J. Choudhary, Mater. Sci. 46 (2011) 6416–6423.
[107] Z. Fan, G. Luo, Z. Zhang, L. Zhou, F. Wei, Mater. Sci. Eng., B 132 (2006) 85–89.
[108] Q. Ling, J. Sun, Q. Zhao, Q. Zhou, Polym. Plast. Technol. Eng. 49 (2010) 481–486.
[109] C.K. Kum, Y.-T. Sung, M.S. Han, W.N. Kim, H.S. Lee, S.-J. Lee, Joo, J. Macromol. Res. 14 (2006) 456–460.
[110] M. Arjmand, M. Mahmoodi, G.A. Gelves, S. Park, U. Sundararaj, Carbon 49 (2011) 3430–3440.
[111] I. Dubnikova, E. Kuvardina, V. Krasheninnikov, S. Lomakin, I. Tchmutin, S.J. Kuznetsov, Appl. Polym. Sci. 117 (2010) 259–272.
[112] J.-M. Thomassin, I. Huynen, R. Jerome, C. Detrembleur, Polymer 51 (2010) 115–121.
[113] N.C. Das, S.J. Maiti, Mater. Sci. 43 (2008) 1920–1925.
[114] U. Basuli, S. Chattopadhyay, C. Nah, T.K. Chaki, Polym. Compos. 33 (2012) 897–903.
[115] U. Basuli, T.K. Chaki, C. Nah, S. Chattopadhyay, Adv. Sci. Lett. 17 (2012) 27–39.
[116] H. Wang, G. Wang, W. Li, Q. Wang, W. Wei, Z. Jiang, S.J. Zhang, Mater. Chem. 22 (2012) 21232–21237.
[117] M.H. Al-Saleh, U. Sundararaj, J. Polym. Sci. Part B: Polym. Phys. 50 (2012) 1356–1362.
[118] J.-M. Thomassin, X. Lou, C. Pagnoulle, A. Saib, L. Bednarz, I. Huynen, R. Jerome, C.J. Detrembleur, Phys. Chem. C 111 (2007) 11186–11192.
[119] Q.-F. Li, Y. Xu, J.-S. Yoon, G.-X. Chen, J. Mater. Sci. 46 (2011) 2324–2330.
[120] M. Mahmoodi, M. Arjmand, U. Sundararaj, S. Park, Carbon 50 (2012) 1455–1464.
[121] M. Arjmand, T. Apperley, M. Okoniewski, U. Sundararaj, Carbon 50 (2012) 5126–5134.
[122] N.J.S. Sohi, M. Rahaman, D. Khastgir, Polym. Compos. 32 (2011) 1148–1154.
[123] M. Ganβ, B.K. Satapathy, M. Thunga, R. Weidisch, P. Pötschke, D. Jehnichen, Acta Mater. 56 (2008) 2247–2261.
[124] M. Mičučik, M. Omastová, I. Krupa, J. Prokeš, P. Pissis, E. Logakis, C. Pandis, P. Pötschke, J.J. Pionteck, Appl. Polym. Sci. 113 (2009) 2536–2551.
[125] A.A. Koval'chuk, V.G. Shevchenko, A.N. Shchegolikhin, P.M. Nedorezova, A.N. Klyamkina, A.M. Aladyshev, Macromolecules, Washington, DC, U.S. 41 (2008) 7536–7542.

Please cite this article in press as: J.-M. Thomassin, et al., Mater. Sci. Eng. R (2013), http://dx.doi.org/10.1016/j.mser.2013.06.001

[126] M.S. Han, Y.K. Lee, W.N. Kim, H.S. Lee, J.S. Joo, M. Park, H.J. Lee, C.R. Park, Macromol. Res. 17 (2009) 863–869.
[127] R.B. Mathur, S. Pande, B.P. Singh, T.L. Dhami, Polym. Compos. 29 (2008) 717–727.
[128] C.-S. Zhang, Q.-Q. Ni, S.-Y. Fu, K. Kurashiki, Compos. Sci. Technol. 67 (2007) 2973–2980.
[129] Z. Liu, G. Bai, Y. Huang, F. Li, Y. Ma, T. Guo, X. He, X. Lin, H. Gao, Y.J. Chen, Phys. Chem. C 111 (2007) 13696–13700.
[130] W.-S. Kim, H.S. Song, B.O. Lee, K.-H. Kwon, Y.-S. Lim, M.-S. Kim, Macromol. Res. 10 (2002) 253–258.
[131] B.P. Singh, Prabha, P. Saini, T. Gupta, P. Garg, G. Kumar, I. Pande, S. Pande, R.K. Seth, S.K. Dhawan, R.B. Mathur, J. Nanopart. Res. 13 (2011) 7065–7074.
[132] C. Basavaraja, E.-A. Jo, B.-S. Kim, D.-S. Huh, Polym. Compos. 32 (2011) 438–444.
[133] S.H. Park, P. Thielemann, P. Asbeck, P.R. Bandaru, Appl. Phys. Lett. 94 (2009) 243113, 243111/243111-243111/.
[134] S.H. Park, P. Theilmann, K. Yang, A.M. Rao, P.R. Bandaru, Appl. Phys. Lett. 96 (2010) 043113, 043115/043111-043115/.
[135] J.S. Im, I.J. Park, S.J. In, T. Kim, Y.-S. Lee, J. Fluorine Chem. 130 (2009) 1111–1116.
[136] I.W. Nam, H.K. Lee, J.H. Jang, Composites, Part A 42A (2011) 1110–1118.
[137] Y. Huang, N. Li, Y. Ma, F. Du, F. Li, X. He, X. Lin, H. Gao, Y. Chen, Carbon 45 (2007) 1614–1621.
[138] N. Li, Y. Huang, F. Du, X. He, X. Lin, H. Gao, Y. Ma, F. Li, Y. Chen, P.C. Eklund, Nano Lett. 6 (2006) 1141–1145.
[139] P. Kuzhir, A. Paddubskaya, D. Bychanok, A. Nemilentsau, M. Shuba, A. Plusch, S. Maksimenko, S. Bellucci, L. Coderoni, F. Micciulla, I. Sacco, G. Rinaldi, J. Macutkevic, D. Seliuta, G. Valusis, J. Banys, Thin Solid Films 519 (2011) 4114–4118.
[140] Z. Ye, Z. Li, J.A. Roberts, P. Zhang, J.T. Wang, G.L. Zhao, J. Appl. Phys. 108 (2010), 054315/054311-054315/054317.
[141] H. Zhang, G. Zeng, Y. Ge, T. Chen, L.J. Hu, Appl. Phys. 105 (2009), 054314/054311-054314/054314.
[142] A. Paddubskaya, D. Bychanok, A. Plyushch, P. Kuzhir, A. Nemilentsau, S. Maksimenko, S. Bellucci, L. Coderoni, F. Micciulla, I. Sacco, G. Rinaldi, J. Macutkevic, D. Seliuta, G. Valusis, J. Banys, J. Nanoelectron. Optoelectron. 7 (2012) 81–86.
[143] J. Macutkevic, D. Seliuta, G. Valusis, R. Adomavicius, P. Kuzhir, A. Paddubskaya, M. Shuba, S. Maksimenko, L. Coderoni, F. Micciulla, I. Sacco, S. Bellucci, Chem. Phys. 404 (2012) 129–135.
[144] W.-S. Jou, H.-Z. Cheng, C.-F. Hsu, J. Electron. Mater. 35 (2006) 462–470.
[145] J. Yun, J.S. Im, H.-I. Kim, Y.-S. Lee, Colloid Polym. Sci. 289 (2011) 1749–1755.
[146] D.A. Makeiff, T. Huber, Synth. Met. 156 (2006) 497–505.
[147] Y.-L. Huang, S.-M. Yuen, C.-C.M. Ma, C.-Y. Chuang, K.-C. Yu, C.-C. Teng, H.-W. Tien, Y.-C. Chiu, S.-Y. Wu, S.-H. Liao, F.-B. Weng, Compos. Sci. Technol. 69 (2009) 1991–1996.
[148] W.-S. Jou, H.-Z. Cheng, C.-F. Hsu, J. Alloys Compd. 434-435 (2007) 641–645.
[149] N.C. Das, Y. Liu, K. Yang, W. Peng, S. Maiti, H. Wang, Polym. Eng. Sci. 49 (2009) 1627–1634.
[150] I.N. Mazov, V.L. Kuznetsov, D.V. Krasnikov, N.A. Rudina, A.I. Romanenko, O.B. Anikeeva, V.I. Suslyaev, E.Y. Korovin, V.A. Zhuravlev, J. Nanotechnol. 648324 (2011) 648327.
[151] J.-M. Thomassin, D. Vuluga, M. Alexandre, C. Jerome, I. Molenberg, I. Huynen, C. Detrembleur, Polymer 53 (2012) 169–174.
[152] Y. Li, C. Chen, J.-T. Li, S. Zhang, Y. Ni, S. Cai, J. Huang, Nanoscale Res. Lett. 5 (2010) 1170–1176.
[153] Y. Li, C. Chen, S. Zhang, Y. Ni, J. Huang, Appl. Surf. Sci. 254 (2008) 5766–5771.
[154] J. Yun, J.S. Im, Y.-S. Lee, H.-I. Kim, Eur. Polym. J. 46 (2010) 900–909.
[155] S.-J. Han, B. Kim, K.-D. Suh, Macromol. Chem. Phys. 208 (2007) 377–383.
[156] H. Jiang, Q. Ni, H. Wang, J. Liu, Polym. Compos. 33 (2012) 1586–1592.
[157] J.-M. Thomassin, I. Molenberg, I. Huynen, A. Debuigne, M. Alexandre, C. Jerome, C. Detrembleur, Chem. Commun. Cambridge, U.K. 46 (2010) 3330–3332.
[158] A.S. Hoang, Adv. Nat. Sci. Nanosci. Nanotechnol. 2 (2011), 025007/025001-025007/025005.
[159] M. Imai, K. Akiyama, T. Tanaka, E. Sano, Compos. Sci. Technol. 70 (2010) 1564–1570.
[160] Y. Yang, M.C. Gupta, K.L. Dudley, R.W. Lawrence, J. Nanosci. Nanotechnol. 5 (2005) 927–931.
[161] I.H. Chen, C.-C. Wang, C.-Y. Chen, J. Phys. Chem. C 114 (2010) 13532–13539.
[162] E.J. Ra, K.H. An, K.K. Kim, S.Y. Jeong, Y.H. Lee, Chem. Phys. Lett. 413 (2005) 188–193.
[163] K.S. Novoselov, A.K. Geim, S.V. Morozov, D. Jiang, Y. Zhang, S.V. Dubonos, I.V. Grigorieva, A.A. Firsov, Science (Washington, DC, U. S.) 306 (2004) 666–669.
[164] J.-S. Moon, D.K. Gaskill, IEEE Trans. Microwave Theory Tech. 59 (2011) 2702–2708.
[165] J. Liang, Y. Wang, Y. Huang, Y. Ma, Z. Liu, J. Cai, C. Zhang, H. Gao, Y. Chen, Carbon 47 (2009) 922–925.
[166] P. Bhattacharya, C.K. Das, S.S. Kalra, J. Mater. Sci. Res. 1 (2012) 126–132.
[167] M. Fang, Z. Tang, H. Lu, S.J. Nutt, Mater. Chem. 22 (2012) 109–114.
[168] C. Basavaraja, W.J. Kim, Y.D. Kim, D.S. Huh, Mater. Lett. 65 (2011) 3120–3123.
[169] Y.-J. Chen, D.D. Nguyen, Y.-A. Li, M.-C. Yip, W.-K. Hsu, N.-H. Tai, Diamond Relat. Mater. 20 (2011) 1183–1187.
[170] H. Yu, T. Wang, B. Wen, M. Lu, Z. Xu, C. Zhu, Y. Chen, X. Xue, C. Sun, M.J. Cao, Mater. Chem. 22 (2012) 21679–21685.
[171] B. Yuan, L. Yu, L. Sheng, K. An, X. Zhao, J. Phys. D: Appl. Phys. 45 (2012) 235106, 235108/235101-235108/.
[172] R. Schueler, J. Petermann, K. Schulte, H.-P. Wentzel, J. Appl. Polym. Sci. 63 (1997) 1741–1746.
[173] L. Flandin, T. Prasse, R. Schueler, K. Schulte, W. Bauhofer, J.Y. Cavaille, Phys. Rev. B: Cond. Matter Mater. Phys. 59 (1999) 14349–14355.
[174] J.-C. Huang, Adv. Polym. Technol. 21 (2002) 299–313.
[175] J.N. Coleman, U. Khan, Y.K. Gun'ko, Adv. Mater. (Weinheim, Ger.) 18 (2006) 689–706.
[176] M. Moniruzzaman, K.I. Winey, Macromolecules 39 (2006) 5194–5205.
[177] Z. Spitalsky, D. Tasis, K. Papagelis, C. Galiotis, Prog. Polym. Sci. 35 (2010) 357–401.
[178] E.T. Thostenson, Z. Ren, T.W. Chou, Compos. Sci. Technol. 61 (2001) 1899–1912.
[179] H. Kim, A. Abdala, C.W. Macosko, Macromolecules (Washington, DC, U. S.) 43 (2010) 6515–6530.
[180] T. Kuilla, S. Bhadra, D. Yao, N.H. Kim, S. Bose, J.H. Lee, Prog. Polym. Sci. 35 (2010) 1350–1375.
[181] J.R. Potts, D.R. Dreyer, C.W. Bielawski, R.S. Ruoff, Polymer 52 (2011) 5–25.
[182] N. Abdel Aal, F. El-Tantawy, A. Al-Hajry, M. Bououdina, Polym. Compos. 29 (2008) 125–132.
[183] C.-Y. Huang, W.-W. Mo, M.-L. Roan, Surf. Coat. Technol. 184 (2004) 163–169.
[184] C.-Y. Huang, W.-W. Mo, M.-L. Roan, Surf. Coat. Technol. 184 (2004) 123–132.
[185] S.S. Tzeng, F.Y. Chang, Mater. Sci. Eng., A A302 (2001) 258–267.
[186] C.Y. Huang, C.C. Wu, Eur. Polym. J. 36 (2000) 2729–2737.
[187] C.-Y. Huang, W.-W. Mo, Surf. Coat. Technol. 154 (2002) 55–62.
[188] C.-Y. Huang, J.-F. Pai, Eur. Polym. J. 34 (1998) 261–267.
[189] C.-Y. Huang, T.-W. Chiou, Eur. Polym. J. 34 (1998) 37–43.
[190] W.-Y. Chiang, K.-Y. Cheng, Polym. Compos. 18 (1997) 748–756.
[191] G. Lu, X. Li, H. Jiang, Compos. Sci. Technol. 56 (1996) 193–200.
[192] C.-Y. Huang, W.-W. Mo, J. Appl. Polym. Sci. 85 (2002) 1661–1668.
[193] W.-Y. Chiang, J.-Y. Ao, J. Polym. Res. 2 (1995) 83–89.
[194] F. El-Tantawy, N. Abdel Aal, Y.K. Sung, Macromol. Res. 13 (2005) 194–205.
[195] C.-C.M. Ma, Y.-L. Huang, H.-C. Kuan, Y.-S. Chiu, J. Polym. Sci. Part B: Polym. Phys. 43 (2005) 345–358.
[196] N. Xie, Q. Jiao, C. Zang, C. Wang, e-Polym. (2009).
[197] H.M. Kim, K. Kim, C.Y. Lee, J. Joo, S.J. Cho, H.S. Yoon, D.A. Pejakovic, J.W. Yoo, A.J. Epstein, Appl. Phys. Lett. 84 (2004) 589–591.
[198] R. Che, L.-M. Peng, X. Duan, Q. Chen, X. Liang, Adv. Mater. (Weinheim, Ger.) 16 (2004) 401–405.
[199] D.-L. Zhao, X. Li, Z.-M. Shen, J. Alloys Compd. 471 (2009) 457–460.
[200] H. Lin, H. Zhu, H. Guo, L. Yu, Mater. Lett. 61 (2007) 3547–3550.
[201] H. Zhu, H. Lin, H. Guo, L. Yu, Mater. Sci. Eng., B 138 (2007) 101–104.
[202] X.-G. Chen, S.-S. Lv, P.-P. Zhang, J.-P. Cheng, S.-T. Liu, Y. Ye, J. Magnet. Magnet. Mater. 324 (2012) 1745–1751.
[203] Q. Su, G. Zhong, J. Li, G. Du, B. Xu, Appl. Phys. A: Mater. Sci. Process. 106 (2012) 59–65.
[204] M.-S. Cao, J. Yang, W.-L. Song, D.-Q. Zhang, B. Wen, H.-B. Jin, Z.-L. Hou, J. Yuan, ACS Appl. Mater. Interf. 4 (2012) 6949–6956.
[205] V.A. Labunov, A.L. Danilyuk, A.L. Prudnikava, I. Komissarov, B.G. Shulitski, C. Speisser, F. Antoni, F. Le Normand, S.L. Prischepa, J. Appl. Phys. 112 (2012) 024309, 024302/024301-024302/.
[206] X. Gui, K. Wang, A. Cao, J. Wei, R. Lv, F. Kang, Q. Shu, Y. Jia, D.J. Wu, Nanosci. Nanotechnol. 10 (2010) 1808–1813.
[207] C. Zhao, A. Zhang, Y. Zheng, J. Luan, Mater. Res. Bull. 47 (2012) 217–221.
[208] A.P. Singh, P. Garg, F. Alam, K. Singh, R.B. Mathur, R.P. Tandon, A. Chandra, S.K. Dhawan, Carbon 50 (2012) 3868–3875.
[209] T. Wang, Z. Liu, M. Lu, B. Wen, Q. Ouyang, Y. Chen, C. Zhu, P. Gao, C. Li, M. Cao, L. Qi, J. Appl. Phys. (Melville, NY, United States) 113 (2013) 024318, 024314/024311-024314/.
[210] X. Sun, J. He, G. Li, J. Tang, T. Wang, Y. Guo, H. Xue, J. Mater. Chem. C: Mater. Opt. Electron. Dev. 1 (2013) 765–777.
[211] E. Ma, J. Li, N. Zhao, E. Liu, C. He, C. Shi, Mater. Lett. 91 (2013) 209–212.
[212] Y.-L. Ren, H.-Y. Wu, M.-M. Lu, Y.-J. Chen, C.-L. Zhu, P. Gao, M.-S. Cao, C.-Y. Li, Q.-Y. Ouyang, ACS Appl. Mater. Interf. 4 (2012) 6436–6442.
[213] P.F. Guan, X.F. Zhang, J.J. Guo, Appl. Phys. Lett. 101 (2012), 153108/153101-153108/153104.
[214] T.T. Tung, J.-F. Feller, T. Kim, H. Kim, W.S. Yang, K.S. Suh, J. Polym. Sci. Part A: Polym. Chem. 50 (2012) 927–935.
[215] L. Li, P. Yih, D.D.L. Chung, J. Electron. Mater. 21 (1992) 1065–1071.
[216] H. Zhao, X. Han, M. Han, L. Zhang, P. Xu, Mater. Sci. Eng., B 167 (2010) 1–5.
[217] L. Deng, M. Han, Appl. Phys. Lett. 91 (2007), 023119/023111-023119/023113.
[218] D.-L. Zhao, X. Li, Z.-M. Shen, Compos. Sci. Technol. 68 (2008) 2902–2908.
[219] X. Feng, G. Liao, J. Du, L. Dong, K. Jin, X. Jian, Polym. Eng. Sci. 48 (2008) 1007–1014.
[220] Y. Cao, Q. Su, R. Che, G. Du, B. Xu, Synth. Met. 162 (2012) 968–973.
[221] T. Zou, H. Li, N. Zhao, C. Shi, J. Alloys Compd. 496 (2010) L22–L24.
[222] T. Bao, Y. Zhao, X. Su, Y. Duan, Mater. Sci. Eng., B 176 (2011) 906–912.
[223] H. Yi, F. Wen, L. Qiao, F.J. Li, Appl. Phys. 106 (2009), 103922/103921-103922/103924.
[224] H. Lin, H. Zhu, H. Guo, L. Yu, Mater. Res. Bull. 43 (2008) 2697–2702.
[225] K.-Y. Park, J.-H. Han, S.-B. Lee, J.-B. Kim, J.-W. Yi, S.-K. Lee, Compos. Sci. Technol. 69 (2009) 1271–1278.
[226] G. Xie, Z. Wang, Z. Cui, Y. Shi, Carbon 43 (2005) 3181–3183.
[227] R. Lv, F. Kang, J. Gu, X. Gui, J. Wei, K. Wang, D. Wu, Appl. Phys. Lett. 93 (2008), 223105/223101-223105/223103.
[228] X. Jin, Q.-Q. Ni, Y. Fu, L. Zhang, T. Natsuki, Polym. Compos. 33 (2012) 317–323.
[229] R. Wang, F. He, Y. Wan, Y. Qi, J. Alloys Compd. 514 (2012) 35–39.
[230] C.Y. Tsay, R.B. Yang, D.S. Hung, Y.H. Hung, Y.D. Yao, C.K. Lin, J. Appl. Phys. 107 (2010), 09A502/501-509A502/503.
[231] Y. Xu, D. Zhang, J. Cai, L. Yuan, W. Zhang, J. Mater. Sci. Technol. (Shenyang, China) 28 (2012) 34–40.
[232] Y.C. Qing, W.C. Zhou, S. Jia, F. Luo, D.M. Zhu, Appl. Phys. A: Mater. Sci. Process. 100 (2010) 1177–1181.

Please cite this article in press as: J.-M. Thomassin, et al., Mater. Sci. Eng. R (2013), http://dx.doi.org/10.1016/j.mser.2013.06.001

[233] X.-Z. Shen, S.-M. Xie, J. Guo, Z.-C. Liu, J. Appl. Polym. Sci. 114 (2009) 3434–3439.
[234] L.-J. Yu, S.H. Ahmad, K. Ing, M.A. Tarawneh, Adv. Mater. Res. (Durnten-Zurich, Switzerland) 501 (2012) 24–28.
[235] S.M. Abbas, R. Chatterjee, A.K. Dixit, A.V.R. Kumar, T.C. Goel, J. Appl. Phys. 101 (2007) 074106, 074105/074101-074105/.
[236] S.M. Abbas, M. Chandra, A. Verma, R. Chatterjee, T.C. Goel, Composites, Part A 37A (2006) 2148–2154.
[237] G. Shen, Z. Xu, Y. Li, J. Magnet. Magnet. Mater. 301 (2006) 325–330.
[238] W. Wang, Q. Li, C. Chang, Synth. Met. 161 (2011) 44–50.
[239] D.-L. Zhao, X. Li, Z.-M. Shen, Mater. Sci. Eng., B 150 (2008) 105–110.
[240] H. Zhu, L. Zhang, L. Zhang, Y. Song, Y. Huang, Y. Zhang, Mater. Lett. 64 (2010) 227–230.
[241] L. Zhang, H. Zhu, Y. Song, Y. Zhang, Y. Huang, Mater. Sci. Eng., B 153 (2008) 78–82.
[242] V. Eswaraiah, V. Sankaranarayanan, S. Ramaprabhu, Nanoscale Res. Lett. 6 (2011) 137.
[243] M. Paligova, J. Vilcakova, P. Saha, V. Kresalek, J. Stejskal, O. Quadrat, Phys. A: Statist. Mech. Appl. (Amsterdam, Netherlands) 335 (2004) 421–429.
[244] J.S. Im, J.G. Kim, S.-H. Lee, Y.-S. Lee, Colloids Surf., A 364 (2010) 151–157.
[245] T.H. Ting, Y.N. Jau, R.P. Yu, Appl. Surf. Sci. 258 (2012) 3184–3190.
[246] A.R.A. Schettini, D. Khastgir, B.G. Soares, Polym. Eng. Sci. 52 (2012) 2041–2048.
[247] C.-Y. Huang, J.-Y. Wu, K.-Y. Tsao, C.-L. Lin, C.-P. Chang, C.-S. Tsai, Y.-H. Chen, J.-T. Yeh, K.-N. Chen, Thin Solid Films 519 (2011) 4765–4773.
[248] Y. Yang, M.C. Gupta, K.L. Dudley, R.W. Lawrence, Adv. Mater. (Weinheim, Ger.) 17 (2005) 1999–2003.
[249] Y. Yang, M.C. Gupta, K.L. Dudley, R.W. Lawrence, Nano Lett. 5 (2005) 2131–2134.
[250] J.-M. Thomassin, C. Pagnoulle, L. Bednarz, I. Huynen, R. Jerome, C. Detrembleur, Mater. Chem. 18 (2008) 792–796.
[251] A. Fletcher, M.C. Gupta, K.L. Dudley, E. Vedeler, Compos. Sci. Technol. 70 (2010) 953–958.
[252] S.P. Mahapatra, V. Sridhar, D.K. Tripathy, Polym. Compos. 29 (2008) 465–472.
[253] V. Eswaraiah, V. Sankaranarayanan, S. Ramaprabhu, Macromol, Mater. Eng. 296 (2011) 894–898.
[254] M.M. Bernal, I. Molenberg, S. Estravis, M.A. Rodriguez-Perez, I. Huynen, M.A. Lopez-Manchado, R.J. Verdejo, Mater. Sci. 47 (2012) 5673–5679.
[255] D.-X. Yan, P.-G. Ren, H. Pang, Q. Fu, M.-B. Yang, Z.-M. Li, J. Mater. Chem. 22 (2012) 18772–18774.
[256] Chen Z., Xu C., Ma C., Ren W., Cheng H.-M. Advanced materials (Deerfield Beach, Fla.) 2013.
[257] H.-B. Zhang, Q. Yan, W.-G. Zheng, Z. He, Z.-Z. Yu, ACS Appl. Mater. Interf. 3 (2011) 918–924.
[258] S.-M. Yuen, C.-C.M. Ma, C.-Y. Chuang, K.-C. Yu, S.-Y. Wu, C.-C. Yang, M.-H. Wei, Compos. Sci. Technol. 68 (2008) 963–968.
[259] S. Pande, B.P. Singh, R.B. Mathur, T.L. Dhami, P. Saini, S.K. Dhawan, Nanoscale Res. Lett. 4 (2009) 327–334.
[260] M. Chen, Y. Zhu, Y. Pan, H. Kou, H. Xu, J. Guo, Mater. Des. 32 (2011) 3013–3016.
[261] J.M. Thomassin, R. Jerome, C. Detrembleur, I. Molenberg, I. Huynen, Phys. Prop. Appl. Poly. Nanocompos. (2010) 563–587.
[262] K.-Y. Park, S.-E. Lee, C.-G. Kim, J.-H. Han, Compos. Sci. Technol. 66 (2006) 576–584.
[263] J.B. Kim, IEEE Trans. Electromag. Comp. (Special Issue on Nanotechnology) 54 (2012) 37–41.
[264] M. Johansson, C.L. Holloway, E.F. Kuester, IEEE Trans. Antennas Propagation 53 (2005) 728–736.
[265] A. Vaziri, Z. Xue, J.W. Hutchinson, J. Mech. Mater. Struct. 1 (2006) 30.
[266] T. Sadowski, J. Bec, Computat. Mater. Sci. 50 (2011) 1269–1275.
[267] A. Alavi Nia, M.Z. Sadeghi, Mater. Des. 31 (2010) 1216–1230.
[268] V. David, I. Nica, A. Salceanu, Proc. Int. Symp. Electromag. Compat. (2009) 4.
[269] H.L. Fan, W. Yang, Z.M. Chao, Compos. Sci. Technol. 67 (2007) 3472–3479.
[270] W.A. Bereuter, D.C. Chang, IEEE Trans. Electromag. Compat. EMC–24 (1982) 58–61.
[271] I. Huynen, N. Quievy, C. Bailly, P. Bollen, C. Detrembleur, S. Eggermont, I. Molenberg, J.M. Thomassin, L. Urbanczyk, T. Pardoen, Acta Mater. 59 (2011) 3255–3266.
[272] P. Bollen, N. Quievy, I. Huynen, C. Bailly, C. Detrembleur, J.M. Thomassin, T. Pardoen, Scripta Materialia 68 (2013) 50–54.
[273] G.D. Seidel, D.C. Lagoudas, J. Appl. Mech. 75 (2008), 041025/041021-041025/041029.

Please cite this article in press as: J.-M. Thomassin, et al., Mater. Sci. Eng. R (2013), http://dx.doi.org/10.1016/j.mser.2013.06.001